JGR Atmospheres

RESEARCH ARTICLE
10.1029/2018JD030214

Determining Factors of Monthly to Decadal Variability in Surface Solar Radiation in China: Evidences From Current Reanalyses

Fei Feng[1] and Kaicun Wang[1]

[1]State Key Laboratory of Earth Surface Processes and Resource Ecology, College of Global Change and Earth System Science, Beijing Normal University, Beijing, China

Key Points:

- All reanalyses overestimate the multiyear mean all-sky R_s over China, which is primarily due to their underestimation of cloud fraction
- 73–12% of the trend biases in all-sky R_s can be explained by trend bias in cloud fraction
- The trend bias in clear-sky-surface solar radiation (a proxy for aerosols) explains 43–30% of the trend bias in R_s

Correspondence to:
K. Wang,
kcwang@bnu.edu.cn

Citation:
Feng, F., & Wang, K. (2019). Determining factors of monthly to decadal variability in surface solar radiation in China: Evidences from current reanalyses. *Journal of Geophysical Research: Atmospheres*, *124*, 9161–9182. https://doi.org/10.1029/2018JD030214

Received 23 DEC 2018
Accepted 1 AUG 2019
Accepted article online 7 AUG 2019
Published online 23 AUG 2019

Abstract Clouds and aerosols play essential roles in regulating surface incident solar radiation (R_s). It has been suggested that the increased aerosol loading over China is a key factor for the decadal variability in R_s and can explain the bias in its trend from reanalyses because the reanalyses do not include the interannual variability of aerosols. In this study, we compare the R_s derived from sunshine duration at 2,400 weather stations in China and that from five reanalyses from 1980 to 2014. The determining factors for the biases in the mean values and trends of R_s from the reanalyses are examined, with the help of R_s and the cloud fraction (CF), from satellite and 2,400 weather stations. Our results show that all reanalyses overestimate the multiyear R_s by 24.10–40.00 W/m^2 due to their underestimations of CF, which is more obvious in southern China. The biases in the simulated CF in the reanalyses can explain the biases in R_s by 55–41%, and the bias in clear-sky surface solar radiation (R_c), which is primarily due to biases in aerosol loading, can explain 32–9% of the bias in R_s. The errors in the trend of the simulated CF can explain the errors in the R_s trends in the reanalyses by 73–12%, and the trend errors in the R_c can explain 43–30% of the trend error in R_s. Our study suggests that more work is needed to improve the simulation of aerosols, clouds, and aerosol-cloud-radiation interactions in the reanalyses.

1. Introduction

Surface incident solar radiation (R_s) is a key component of the surface energy budget. It drives the global climate system and the hydrological and carbon cycles (*C*. Dorno, 1920; Roderick & Farquhar, 2002; Sedlar, 2018; Sellers et al., 1990; Wang et al., 2017). Widespread solar radiation measurements have shown that R_s has significant decadal variability, which is known as *global dimming* (from the 1950s to 1980s) and *brightening* (since the mid-1980s, Wild, 2009). The variation in R_s is closely related to climate change and global warming (Ruosteenoja & Raisanen, 2013). This has been regarded as an important driver of the observed decadal variability of hemisphere and global mean surface temperature during the last century (Ramanathan et al., 2005; Ruckstuhl et al., 2008; Wang & Dickinson, 2013; Wild, 2009).

Clouds and aerosols have been considered the main contributors to the variability in R_s (Bodas-Salcedo et al., 2014; Folini & Wild, 2011; Ghan et al., 2012; Pyrina et al., 2015; Tang et al., 2012; Wang et al., 2012). It is argued that the reduction in aerosol loading is the primary factor of R_s brightening from 1980 to 2014 over Europe (Nabat et al., 2015). However, studies based on satellite retrievals have found that the reason for the increasing trend in R_s from 1992 to 2015 over Europe is the decrease in the cloud fraction (CF, Pfeifroth et al., 2018). Augustine and Dutton (2013) found that the increasing trend in R_s is mainly due to a decrease in CF over the United States from 1996 through 2011.

Changes in aerosol loading have been reported to be the primary cause of variations in R_s over China (Che et al., 2005; J. Li et al., 2018; Liang & Xia, 2005; Qian et al., 2015; Xia, 2010). For example, Li et al. (2018) find that aerosol loading was the most likely major cause of variations in R_s from 2005 to 2015 over China, especially for the northeast and southern parts of China. In contrast, Tang et al. (2017) conclude that clouds and the interactions between clouds and aerosols are the main reasons for the variation in R_s.

The above-mentioned studies on the attributions of the trend in R_s to clouds and aerosols are primarily qualitative due to limited numbers of surface measurements of R_s, CF, and aerosol loading. Observations of R_s are sparsely distributed and have limited spatial and temporal coverage (Wild, 2016). Moreover, the solar radiation measurements over China suffer from problems such as sensitivity drift and instrument

replacement (Wang, 2014; Wang et al., 2015; Yang et al., 2018; Zhang & Lu, 1988, 1990). Sunshine duration (SunDu) records have been suggested that can be used to reconstruct long-term R_s with comparatively large spatial coverage (He et al., 2018; Matuszko, 2014; Sanchez-Lorenzo et al., 2008; Wang et al., 2015b; Yang et al., 2006). Satellite-derived R_s products also provide an estimate of R_s (Feng & Wang, 2018b; Li et al., 2017; Ma et al., 2015). More importantly, satellite data provide CF in addition to the ground-based manual observations of CF.

Compared with observations and satellite data, the R_s reanalysis data have complete spatial and temporal coverage by combining observations and forecast models. The radiative fluxes from the reanalyses are widely used as forcing data in many climate models (Essou et al., 2017). However, R_s reanalyses contain substantial biases (Slater, 2016; Wang et al., 2015; Wu et al., 2015) due to the uncertainties in clouds and aerosols in the reanalyses (Fujiwara et al., 2017). Complete knowledge of the interactions among clouds, aerosols and radiation, and the related parameterizations in the climate models or reanalyses can help to reduce the uncertainty in predicting potential future climate changes, especially at regional scales (Loew et al., 2016; Zadra et al., 2018).

In this study, we compare the R_s, CF from five current reanalyses with field observations, satellite retrievals, and the satellite and reanalyses-derived clear-sky surface solar radiation (R_c), which is closely related to aerosols, by analyzing the climatologies, spatial patterns, seasonal variations, and trends in R_s, CF, and R_c from these reanalyses. Second, we evaluate the relationship between the bias in R_s and those in the CF and R_c. These analyses help to figure out the determining factors of monthly to decadal variability in surface solar radiation in the reanalysis system and observations in China from 1980 to 2014.

2. Data and Methodology

2.1. Ground-Based Observations

SunDu from 1980 to 2014 are collected from approximately 2,400 China Meteorological Administration (CMA) weather stations (http://data/cma/cn/data, Figure 1). These SunDus are then used to calculate the monthly mean R_s following the method of the revised Ångström-Prescott equation (1, Wang, 2014; Wang et al., 2015; Yang, Koike, & Ye, 2006).

$$\frac{R_s}{R_c} = a_0 + a_1\frac{n}{K} + a_2\left(\frac{n}{K}\right)^2 \tag{1}$$

$$R_c = \int I \cdot T_b \cdot \sin(h) \cdot \mathrm{d}t + \int I \cdot T_d \cdot \sin(h) \cdot \mathrm{d}t \tag{2}$$

where n represents the measured sunshine duration and K represents the theoretical value of the sunshine duration. a0, a1, and a2 are determined following the method of Wang (2014). R_c is the daily total solar radiation under clear sky. I is solar irradiance at the top of the atmosphere. T_b and T_d denote atmospheric transmittance for direct solar radiation and diffuse solar radiation. h is the solar elevation.

Existing studies (Manara et al., 2015; Sanchezlorenzo et al., 2013; Tang et al., 2011; Wang et al., 2012; Yang et al., 2018) have shown that SunDu-derived R_s is a reliable R_s proxy data set at time scales ranging from monthly to decadal that can reflect the impacts of aerosols and clouds on R_s over China. SunDu data are relatively widely distributed and have a long time record, which extends from the late nineteenth century to the present (Sanchez-Lorenzo et al., 2009; Wild, 2009).

Moreover, R_s measurements such as pyranometers require careful calibrations (Wood et al., 2015; Yang et al., 2018) due to the thermal offsets (Philipona, 2002; Zo et al., 2017) and the directional response errors (Myers et al., 2002). Moreover, R_s measurements are sparsely distributed in China. In spite of uncertainty in short time scales, SunDu-derived R_s data have their advantage in quantifying annual to decadal variability of R_s (Feng & Wang, 2018a; Wang, 2014).

We also collected synoptic observations of the total CF from 2,400 weather stations, which are collocated with the SunDu measurement sites. Daily observational total cloud amounts (in tenths), which are observed by human eyes 4 times a day (2:00, 8:00, 14:00, and 20:00) based on the specifications for surface

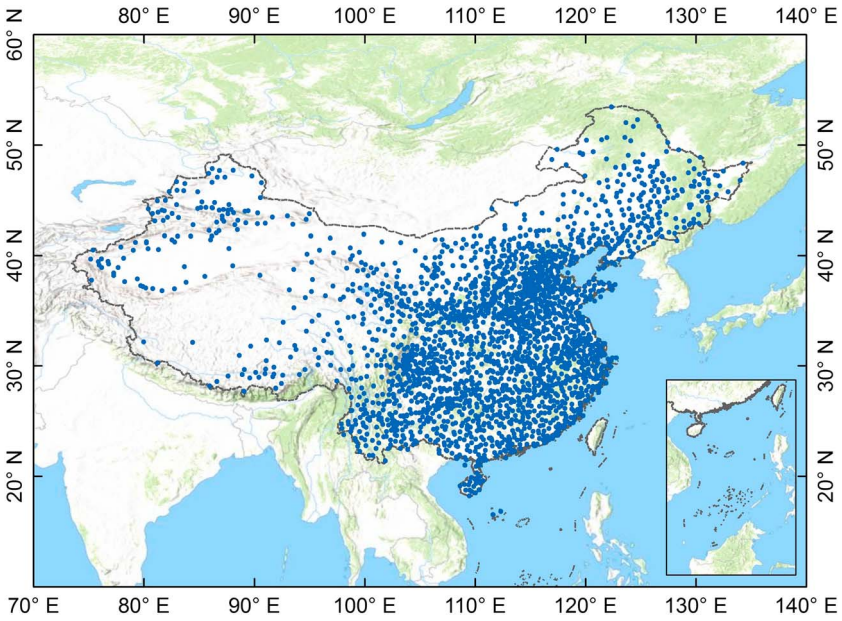

Figure 1. The 2,400 meteorological sites used in this study. The based hillshade map was produced by an elevation map of China using the global digital elevation model (DEM) derived from the Shuttle Radar Topography Mission 30 (SRTM30) data set.

meteorological observation, are collected and then averaged to get monthly mean observed cloud amount and are linearly converted into the percentage scale to enable comparison with the reanalysis data.

2.2. Satellite Data

R_s data from the latest release of the Clouds and the Earth's Radiant Energy System energy balanced and filled product (CERES EBAF) surface product (edition 4) and cloud amounts from the CERES Synoptic (CERES SYN1deg) edition 4 product are collected in this study (Kato et al., 2018). CERES is a radiometer on board the Tropical Rainfall Measuring Mission, Terra, Aqua, and Suomi National Polar-orbiting Partnership satellites and National Oceanic and Atmospheric Administration-20. CERES measures three filtered radiances, including shortwave (0.3–5 μm), total (0.3–200 μm), and window (8–12 μm).

The CERES-EBAF product provides global monthly mean R_s data. The input cloud properties for CERES EBAF, such as optical thickness and emissivity from Moderate Resolution Imaging Spectradiometer (MODIS) and geostationary satellites, are constrained by a cloud profiling radar, Cloud-Aerosol Lidar and Infrared Pathfinder Satellite Observations detectors, and CloudSat. MODIS collection 5-derived aerosol data are used as input data for the CERES EBAF product. R_s of CERES EBAF is produced with a radiative transfer model constrained by CERES observations at the top of the atmosphere (Kato et al., 2018).

Compared with the previous version of CERES EBAF (Ed2.8), the newly released product (version 4.0) has extensive improvements in the inputs and algorithms. For example, the newly released version 4.0 product eliminated the discontinuities in the temperature and humidity time series at the beginning of 2008. Furthermore, the biases in temperature and specific humidity from the Goddard Earth Observing System (GEOS) version 5.4.1 reanalysis are corrected using atmospheric infrared sounder data. All the improvements help to improve its capability in quantifying long-term trend of R_s. The uncertainties of CERES EBAF data, reported by Kato et al. (2018), in all-sky global annual mean R_s is 4 W/m^2. The new CERES products are supplemented with geostationary satellite data between the twice-per-day passes to document diurnal variation of solar and IR irradiance overcoming a major flaw in polar orbiter (i.e., CERES) data.

Existing studies (Feng & Wang, 2018b; Ma et al., 2015; Wang et al., 2015) also show that the CERES EBAF surface product provides reliable estimations of monthly R_s. Feng and Wang (2018a) find that CERES EBAF has a bias of 7.94 W/m^2 compared with observation and 7.53 W/m^2 compared with SunDu-derived R_s from 2000 to 2014. The comparison results of CERES EBAF, GEWES-SRB, and ISCCP-FD-SRF from Li, Xin, and

Table 1
Summary of the Parameterizations and Variables in the Reanalyses

	Model	Spatial resolution	Assimilation scheme	Reference
ERAI	IFS Cycle 31r2	TL255 (~79 km)	4D-Var	Dee et al. (2011)
JRA55	JMA GSM	TL319 (~55 km)	4D-Var	Kobayashi et al. (2015)
MERRA2	GEOS 5.12.4	0.5° × 0.625°	3D-FGAT	Gelaro et al. (2017)
MERRA	GEOS 5.0.2	0.5° × 0.667°	3D-FGAT	Rienecker et al. (2011)
CFSR	NCEP GFS	0.3125° × 0.3125°	3D-FGAT	S. Saha et al. (2010) and Suranjana Saha et al. (2014)

Note. The 3D-Var (4D-Var) is the three-dimensional (four-dimensional) variational assimilation system, and FGAT is the first guess at the appropriate time. GSM is the global spectral model. MERRA = Modern-Era Retrospective Analysis for Research and Applications; JRA55 = Japanese 55-year reanalysis; ERAI = European Centre for Medium Range Weather Forecasting Reanalysis-Interim; CFSR = Climate Forecast System Reanalysis.

Peng (2017) show that CERES EBAF have lowest root-mean-square error (RMSE, 14.73 W/m^2) compare with solar radiation measurements in China.

2.3. Reanalysis Data

Five of the latest global reanalysis products, including the European Centre for Medium Range Weather Forecasting Reanalysis-Interim (ERAI), Japanese 55-year reanalysis (JRA55), Climate Forecast System Reanalysis (CFSR), Modern-Era Retrospective Analysis for Research and Applications version 2 (MERRA2) and MERRA, were collected in this study. The brief descriptions of these five reanalyses are summarized in Table 1. It is necessary to note that the time span of the CFSR is from 1979 to 2010. We use its successor, version 2 (CFSR2), to provide the subsequent CFSR estimates from 2010 to 2014 according to previous studies, in which CFSR2 has been used as a continuation of CFSR due to few changes in the physical models (*Suranjana* Saha et al., 2014). ERAI does not provide a R_c product, and we calculate the R_c from its albedo and surface net solar radiation products for a clear sky.

These five reanalyses do not assimilate any R_s data from conventional or satellite observations. R_s derived from these reanalyses is calculated using radiation transfer models. Specifically, the ERAI used a six-band shortwave parameterization model developed by Fouquart and Bonnel (1980). JRA55 used a shortwave parameterization model developed by Briegleb (1992). The shortwave parameterization of the CFSR is based on the Rapid Radiative Transfer Model for General Circulation Models developed by Clough et al. (2005). Both MERRA2 and MERRA applied the Goddard climate and radiation package (CLIRAD) for shortwave parameterization (Fujiwara et al., 2017).

The simulation of the CF in reanalyses falls into two categories: (1) the diagnostic scheme and (2) the prognostic scheme. CF in the diagnostic scheme is parameterized by an empirical function of relative humidity or a probability density function (PDF) of moisture variability. In the prognostic scheme, the CF is calculated using a prognostic equation of the sources and sinks of cloud areas. For the reanalyses, the CF from the ERAI is calculated using a prognostic scheme (Berrisford et al., 2009). CFSR uses a diagnosed scheme for CF computation (Saha et al., 2006). JRA55 uses a PDF-based diagnosed cloud scheme (Smith, 2010). MERRA applies a prognostic cloud scheme (Bacmeister et al., 2006), and MERRA2 updates its atmospheric model, which results in increasing cloud condensation that has a substantial impact on CF simulation (Molod et al., 2015).

ERAI, CFSR, MERRA2, and MERRA use a maximum-random overlap scheme to depict different vertical layers with cloud overlap, whereas the JRA55 uses a random overlap scheme. Climatological aerosol values are used in the ERAI, CFSR, JRA55, and MERRA. MERRA2 uses analyzed aerosol values (Randles et al., 2017), which are produced by the Global Ozone Chemistry Aerosol Radiation and Transport model, and assimilates satellite-derived Aerosol Optical Depth (AOD) values and Aerosol Robotic Network AOD values.

2.4. Methods

We assess the R_s values and CF, from the reanalyses by comparing them with surface observations and satellite retrievals. Both satellite retrievals and field observations are used as all-sky R_s reference. Clear-sky surface solar radiation (R_c), which is closely related to atmospheric aerosol loading, can be calculated with input from reanalyses and satellite. R_c from reanalyses were also compared with satellite retrievals to illustrate the impact of aerosols.

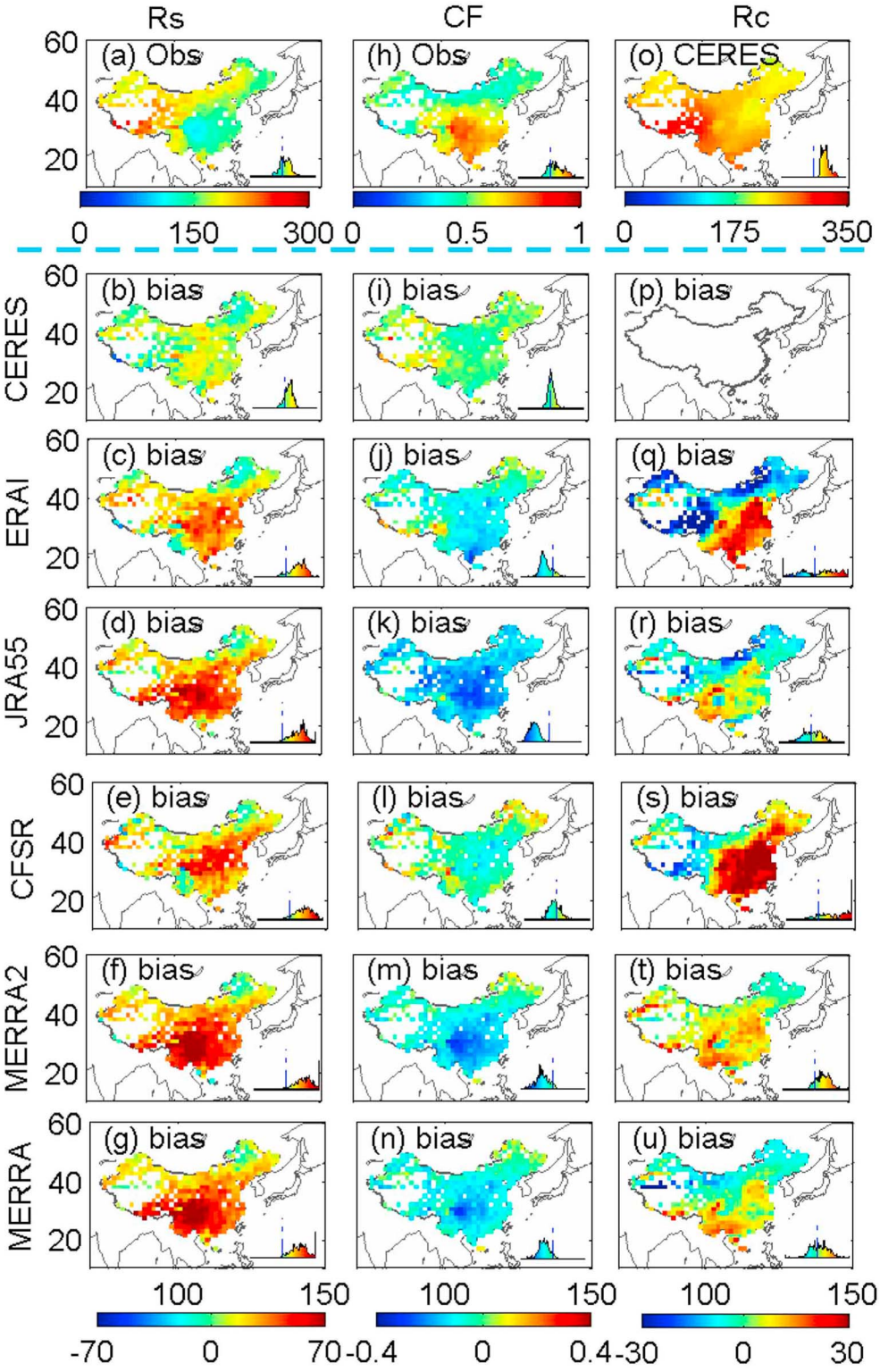

Figure 2. Spatial distribution of multiyear mean monthly surface solar radiation (R_s), cloud fraction (CF), and the surface solar radiation under clear-sky condition (R_c) from 2000 to 2014. The first line (a, h, o) shows the observed multiyear mean monthly R_s, CF and CERES EBAF-derived R_c from 2000 to 2014; the rest of the lines show the results of the multiyear mean monthly R_s, CF, and R_c from the reanalyses minus the multiyear mean monthly R_s, CF, and R_c from the observations and CERES data. The probability density plot represents the distribution of multiyear mean monthly R_s, CF, and R_c (a, h, and o subplots) and the distribution of the CERES and reanalyses corresponding biases (rest subplots) in each subplot, and the values are consistent with the colorbar range. CERES EBAF = Clouds and the Earth's Radiant Energy System energy balanced and filled product.

Table 2
Evaluations of the Surface Incident Solar Radiation (R_s), Cloud Fraction (CF), and Surface Incident Solar Radiation Under Clear Condition (R_c) From the Reanalyses Using 2,400 Field Observations and the CERES EBAF Data (CERES)

	Typ	Ref	R^2	Bias	MAB	Std	RMSE
CERES	R_s	Obs	0.96	8.22	13.43	9.90	15.71
ERAI	R_s	Obs	0.89	24.13	28.09	15.96	30.94
JRA55	R_s	Obs	0.93	34.02	35.33	14.66	37.09
CFSR	R_s	Obs	0.89	27.78	31.90	18.40	35.15
MERRA2	R_s	Obs	0.89	40.02	41.48	16.92	43.20
MERRA	R_s	Obs	0.87	38.35	39.78	18.42	42.00
ERAI	R_s	CERES	0.89	16.38	20.66	16.11	24.83
JRA55	R_s	CERES	0.91	26.26	28.49	16.81	32.58
CFSR	R_s	CERES	0.89	20.18	25.91	19.25	30.62
MERRA2	R_s	CERES	0.87	32.19	34.30	18.81	38.63
MERRA	R_s	CERES	0.85	30.39	33.09	20.71	38.12
ERAI	CF	Obs	0.67	−0.09	0.11	0.08	0.12
JRA55	CF	Obs	0.62	−0.18	0.19	0.08	0.17
CFSR	CF	Obs	0.64	−0.03	0.09	0.08	0.13
MERRA2	CF	Obs	0.47	−0.13	0.15	0.11	0.15
MERRA	CF	Obs	0.53	−0.11	0.14	0.10	0.12
ERAI	CF	CERES	0.70	−0.09	0.11	0.07	0.12
JRA55	CF	CERES	0.64	−0.19	0.19	0.07	0.21
CFSR	CF	CERES	0.66	−0.03	0.08	0.08	0.10
MERRA2	CF	CERES	0.53	−0.13	0.15	0.09	0.17
MERRA	CF	CERES	0.56	−0.11	0.13	0.09	0.15
ERAI	R_c	CERES	0.96	1.19	20.42	17.57	24.96
JRA55	R_c	CERES	0.98	0.00	10.45	9.10	12.70
CFSR	R_c	CERES	0.98	16.62	22.46	14.65	25.47
MERRA2	R_c	CERES	0.99	7.27	10.42	8.99	12.75
MERRA	R_c	CERES	0.99	1.86	10.36	9.58	12.61

Note. All statistics are calculated by the original values. MAB, Std, and RMSE represent the mean absolute bias, standard deviation, and root-mean-square error, respectively. CERES EBAF = Clouds and the Earth's Radiant Energy System energy balanced and filled product; MERRA = Modern-Era Retrospective Analysis for Research and Applications; JRA55 = Japanese 55-year reanalysis; ERAI = European Centre for Medium Range Weather Forecasting Reanalysis-Interim; CFSR = Climate Forecast System Reanalysis.

To eliminate the impact of surface observations distribution inhomogeneities, we interpolate the field observations into 1° × 1° grid cells using the area-weighted averaging method (Du et al., 2018). To be specific, we divide the study region into 1° × 1° grids covering China and assigned all sites to the grids. For a certain grid contained more than one site, the area-weighted average of these sites are calculated as this grid value. For consistency, all data are transformed into 1° × 1° grids based on the bilinear interpolation method.

The spatial distributions of the multiyear mean R_s, CF, and R_c over China, along with the biases in these parameters from the reanalyses, are analyzed in this study. The linear trends in R_s, CF, satellite-derived R_c, and R_c from reanalyses are calculated by the least squares method. The trends are evaluated using observations and satellite retrievals. To ensure consistent comparisons, all the trends are also calculated by using 1° × 1° grids data including sites observation. To quantify the impacts of CF on all-sky R_s error between the reanalysis data and observations, correlation coefficients (R) of linear regression plots between CF error and all-sky R_s error are calculated. It is essential to assess the sensitivity of error in simulated R_s to CF and R_c. Therefore, we calculated a polynomial regression model to analyze the sensitivity of R_s to the biases in the CF and R_c

$$\Delta R_s = \beta_i \Delta x_i + m + \varepsilon \tag{2}$$

where β_i represents the sensitivity, which is the slope of the linear regression line between the bias in R_s plotted against the bias in x_i. Δx_i represents the bias in the annual anomaly for the related variable (e.g., CF and R_c). ΔRs represents the bias in the annual anomaly R_s, and m and ε represent the constant and

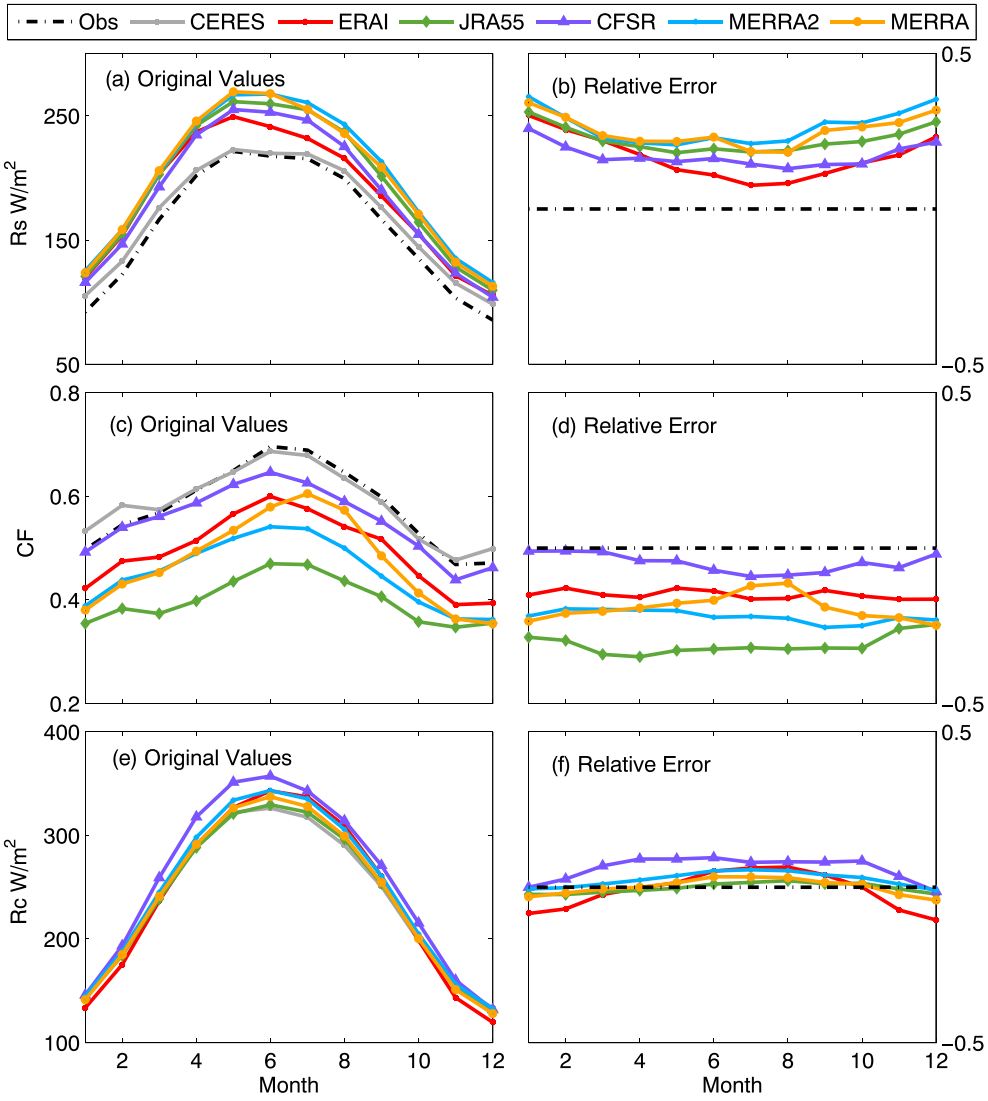

Figure 3. Seasonal variations in the surface solar radiation (R_s), cloud fraction (CF), and the surface solar radiation under clear-sky condition (R_c). The first column (a, c, and e) shows the national mean values for each month using all site data. The second column (b, d, and f) shows the relative bias for each month. The reference for the R_c data is calculated using the CERES EBAF data. CERES EBAF = Clouds and the Earth's Radiant Energy System energy balanced and filled product.

residual, respectively. The coefficient of determination (R^2) of those linear plots is used to determine the degree to which Δx_i explain the variability of ΔRs. The R_s trend errors are calculated as follows:

$$\delta = \frac{\beta_i \Delta T_{x_i}}{\Delta T_{R_s}} \times 100\% \tag{3}$$

where δ represents the sensitivity in the trend error and ΔT_{x_i} represents the trend error in the annual anomaly for the related variable (e.g., CF and R_c). ΔT_{R_s} represents the trend error in the annual anomaly R_s, and β_i is calculated using equation (2). The national mean sensitivity in the trend error is calculated by the mean of absolute values.

3. Results

3.1. Multiyear Mean R_s, CF, and R_c Over China

Figure 2 shows the multiyear means of R_s, CF, and R_c and their biases in the reanalyses from 2000 to 2014. Based on the field observations, R_s is higher in Tibet and western China, with an approximate range of

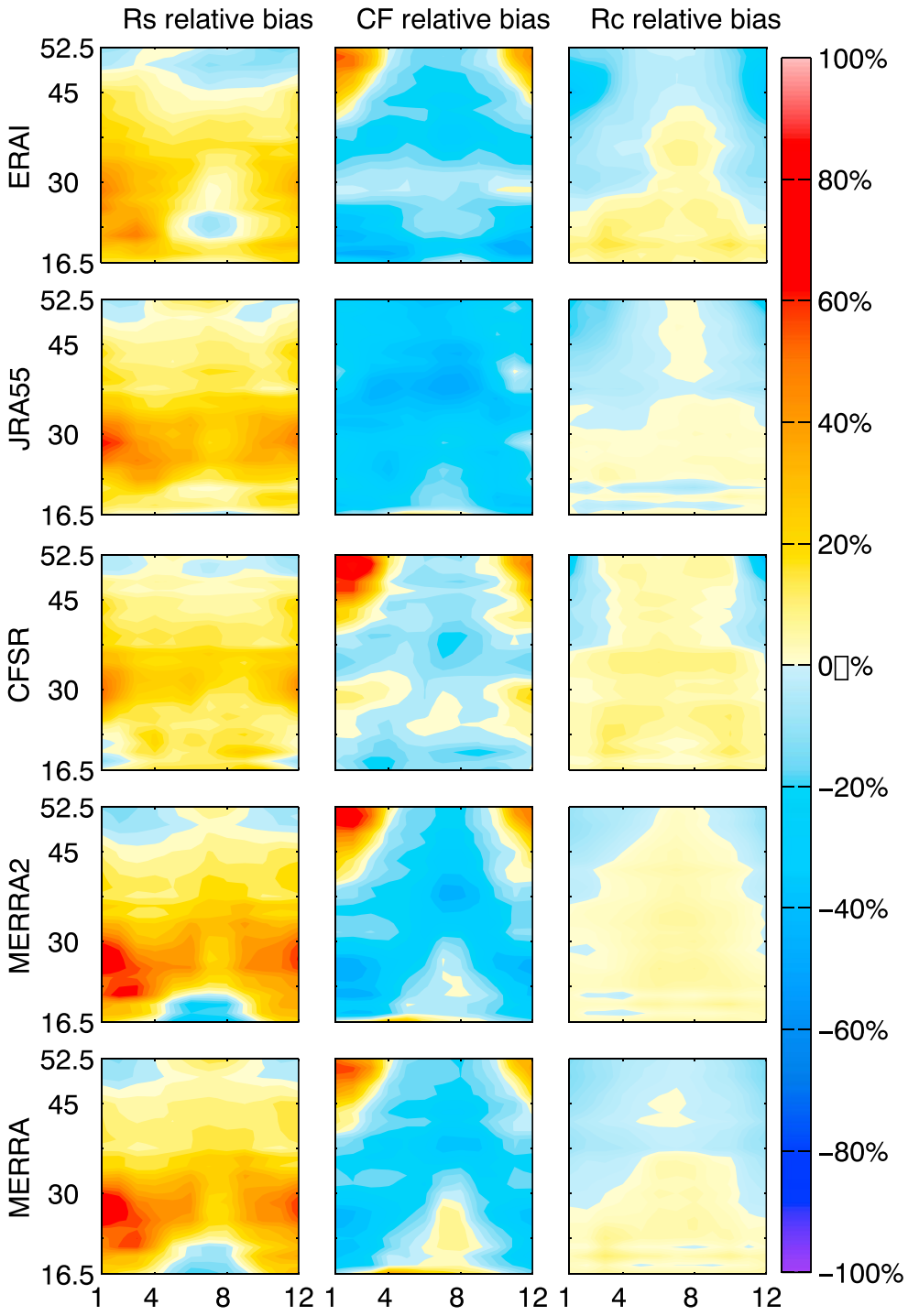

Figure 4. Seasonal variations in the relative bias in zonal mean surface solar radiation (R_s), cloud fraction (CF), and the surface solar radiation under clear-sky condition (R_c). The horizontal axis represents months, and the vertical axis represents latitude. The reference data for R_s and CF are based on the observed data, and the R_c reference data are calculated using the CERES EBAF data. CERES EBAF = Clouds and the Earth's Radiant Energy System energy balanced and filled product.

180–300 W/m^2, and lower in eastern China and southern China, ranging from approximately 120 to 180 W/m^2. The observed CF generally exhibits a reversed spatial pattern, with high values in southern China (0.6–1) and low values in northern China (0.4–0.6). R_c over the Tibetan Plateau (300–340 W/m^2) is

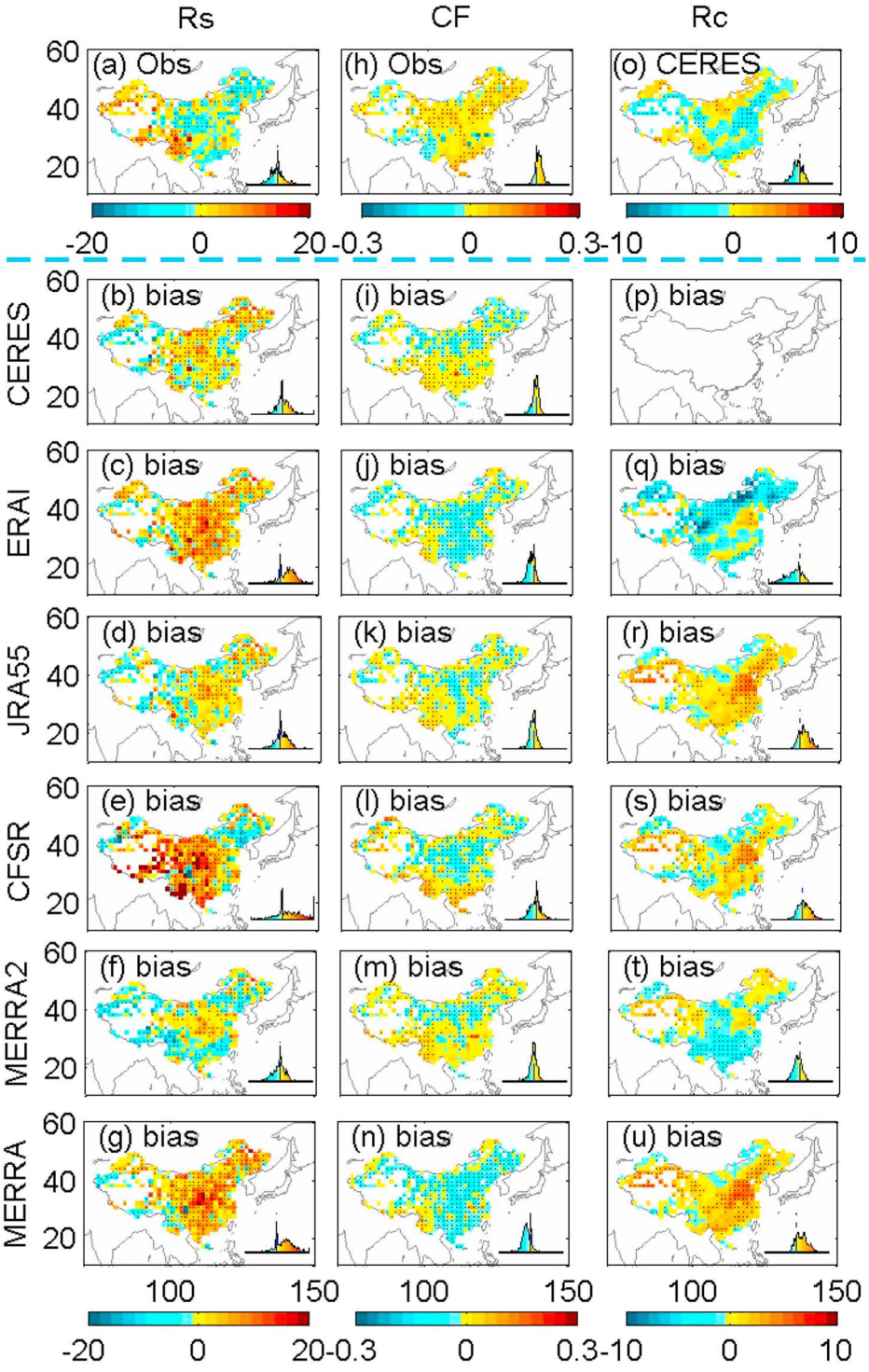

Figure 5. Spatial distributions of monthly anomaly trends (per decade) of surface solar radiation (R_s), cloud fraction (CF), and the surface solar radiation under clear-sky condition (R_c) from 2000 to 2014. The first line (a, h, o) shows the monthly anomaly trends (per decade) of the observed R_s, observed CF, and CERES EBAF-derived R_c from 2000 to 2014; the rest of the lines show the results of the monthly anomaly trends (per decade) of R_s and CF from the reanalyses minus those of R_s, CF, and R_c from the observations. Mann-Kendall analysis are used to establish the significance of trends. The black dots on the maps represent significant trends. The probability density plot embedded in each subplot is the same with Figure 2 but stands for the distribution of monthly anomaly trends (a, h, and o subplots) and the distribution of monthly anomaly trends bias of the CERES and reanalyses (rest subplots). CERES EBAF = Clouds and the Earth's Radiant Energy System energy balanced and filled product.

Table 3
Statistical Summary of the Linear Trends (10 years) in the Monthly Anomaly Surface Solar Radiation (R_s), Cloud Fraction (CF), and the Surface Solar Radiation Under Clear-Sky Condition (R_c) Anomalies Given the National Mean Over China

	2000–2014			1980–2014	
	R_s	CF (tenfold)	R_c	R_s	CF (tenfold)
Obs	−0.89 (−0.03 to 0.01)	**0.21 (0.00–0.00)**		**−0.72 (−0.01–0.00)**	**0.04** (0.0–0.00)
CERES	−0.64 (−0.03 to 0.01)	0.02 (0.00–0.00)	**−0.88 (−0.02 to 0.00)**		
ERAI	**3.95 (0.01–0.05)**	−0.14 (0.00–0.00)	**−3.09 (−0.04 to −0.02)**	**1.46 (0.01–0.02)**	**−0.07 (0.0–0.00)**
JRA55	−0.13 (−0.01 to 0.01)	0.01 (0.00–0.00)	0.26 (0.00–0.00)	0.42 (0.00–0.01)	−0.03 (0.0–0.00)
CFSR	**4.80 (0.02–0.06)**	0.01 (0.00–0.00)	**−0.38 (−0.01 to 0.00)**	**3.33 (0.02–0.03)**	**−0.11 (0.0–0.00)**
MERRA2	**−2.25 (−0.03 to −0.01)**	0.06 (0.00–0.00)	**−1.71 (−0.02 to −0.01)**	**−0.87 (−0.01 to 0.00)**	**−0.09 (0.0–0.00)**
MERRA	**4.17 (0.02–0.04)**	**−0.26 (0.00–0.00)**	**0.58 (0.00–0.01)**	**1.18 (0.01–0.01)**	**−0.11 (0.0–0.00)**

Note. Mann- Kendall analysis are used to establish the significance of trends. Numbers in the parentheses represent uncertainties by Sen's nonparametric estimator. Cloud fraction trends and their uncertainties are increased tenfold times because the original values are too small for CF. Bold numbers represent significance of trends. CERES = Clouds and the Earth's Radiant Energy System; MERRA = Modern-Era Retrospective Analysis for Research and Applications; JRA55 = Japanese 55-year reanalysis; ERAI = European Centre for Medium Range Weather Forecasting Reanalysis-Interim; CFSR = Climate Forecast System Reanalysis.

larger than that over other regions of China (180–260 W/m^2, Figure 2), and the variation in R_c in the Tibetan Plateau is small due to its high altitude, low aerosol loading and water vapor concentration, not to mention the low value center for total column ozone over the Tibetan Plateau (Zhou et al., 2006).

R_s is estimated by ground observations, and the CERES EBAF shows good agreements, with a low mean absolute bias (MAB) = 13.43 W/m^2, R^2 = 0.96, and RMSE = 15.71 W/m^2. The biases in CERES EBAF show a nearly homogeneous spatial distribution (Figure 2). These good agreements can also be seen the CF from the CERES EBAF data. Using field observations as a reference, all five reanalyses significantly overestimate the multiyear mean R_s over China as follows: ERAI, JRA55, CFSR, MERRA2, and MERRA with MAB equal to 28.09, 35.33, 31.90, 41.48, and 39.78 W/m^2, respectively (Table 2). Correspondingly, CF are underestimated by five reanalyses as follows: ERAI, JRA55, CFSR, MERRA2, and MERRA with MAB equal to 0.11, 0.19, 0.09, 0.15, and 0.14, respectively, especially in the Sichuan basin (103–108°E, 28–32°N). The R_c MAB values for ERAI, JRA55, CFSR, MERRA2, and MERRA are as follows: 20.42, 10.45, 22.46, 10.42, and 10.36 W/m^2, respectively. Similar results can also be found in the distribution diagrams of Figure 2.

Reanalyses R_s display larger relative biases in winter and early spring than those in other seasons (Figure 3). The zonal mean relative biases in R_s, CF, and R_c are shown in Figure 4. The spatial patterns of the relative bias in R_s further indicate that large biases in winter and spring mainly occur in the area between 25 and 30°N. The relative bias in the CF shows an opposite spatial pattern compared with that in R_s, especially via MERRA and MERRA2. The R_c estimated by the reanalyses exhibits an overall low relative bias for different seasons.

3.2. Trends of R_s, CF, and R_c Over China

The trends in R_s, CF, and R_c over China from 2000 to 2014 and the corresponding biases via the satellite and reanalyses are shown in Figure 5. Generally, observed R_s shows a national mean trend of −0.89 W/m^2 per decade (Table 3). The observed CF shows an overall increasing trend (0.02 per decade). The national mean decreasing trend in R_s and the national mean increasing trend in CF can also be seen during the period of 1980–2014. In spatial terms, most of China shows a slight decreasing trend in R_s (Figure 5). The increasing trend in R_s is comparatively high in southwest China. Conversely, the increasing trend in the CF can be seen in many parts of China, except in southwest China. Based on the CERES EBAF data, the R_c shows a decreasing trend in eastern China and an increasing trend in north China. Moreover, the distribution diagrams of Figure 5 indicate that reanalyses have more positive R_s trend bias and negative CF trend bias. Based on the CERES EBAF data, the national mean trend in R_c from 2000 to 2014 is −0.88 W/m^2 per decade.

Compared with the reanalyses, the CERES EBAF shows a more consistent national mean R_s trend and CF trend with those of the ground observations (Table 3). All reanalyses show poor performance in simulating

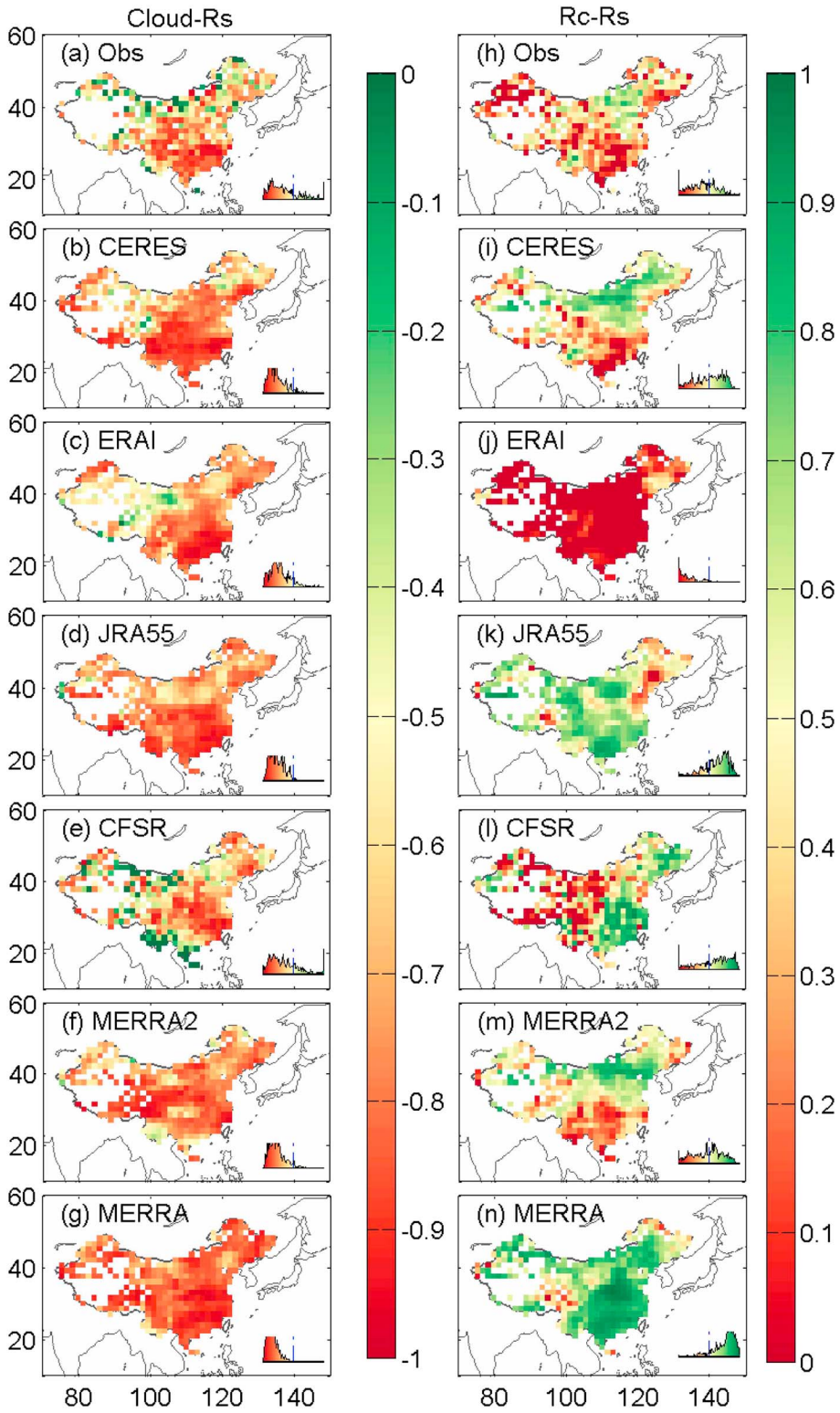

Figure 6. The spatial distributions of the correlation coefficient (R). (a–g) The R between the annual anomaly surface incident solar radiation (R_s) and the annual anomaly cloud fraction (CF). (h–n) The R between the annual anomaly R_s and the annual anomaly the R_c. Obs denotes the observation data, and CERES denotes the CERES EBAF surface data. The probability density plot embedded in each subplot is the same with Figure 2 but stands for the distribution of correlation coefficient. CERES EBAF = Clouds and the Earth's Radiant Energy System energy balanced and filled product.

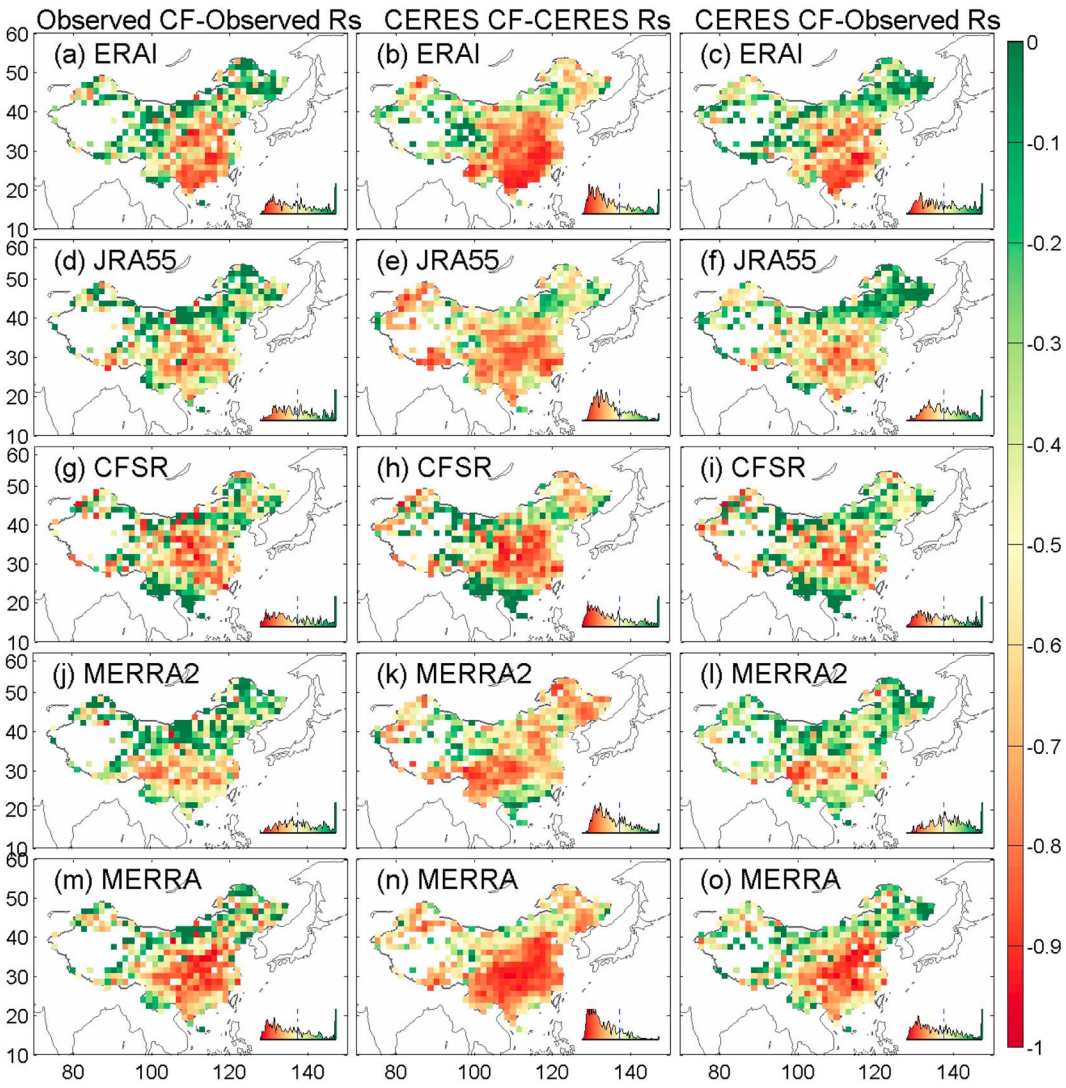

Figure 7. Maps of the correlation coefficient (R) between the bias in the annual anomaly cloud fraction (CF) and the bias in the annual anomaly surface solar radiation (R_s). In the left column (a, d, g, j, and m), the observed CF and the observed R_s represent the CF reference data derived from the observations, and the R_s reference data are the SunDu-derived R_s data. In the middle column (b, e, h, k, and n), CERES CF and CERES R_s represent the CF reference data and R_s reference data are calculated by the CERES EBAF data. In the right column (c, f, i, l, and o), CERES CF and observed R_s represent the CF reference data and the CERES EBAF data, and the R_s reference data are the SunDu-derived R_s data. The time span is from 2000 to 2014. The probability density plot embedded in each subplot is the same with Figure 2 but stands for the distribution of correlation coefficient. CERES EBAF = Clouds and the Earth's Radiant Energy System energy balanced and filled product.

CF trends and R_c trends compared with the CERES EBAF data (Table 3 and Figure 5). ERAI and MERRA produce large, positive R_s trend biases ranging from 10 to 20 W/m^2 per decade and correspondingly large negative CF trend biases (0 to −0.3 per decade) in east China. For R_c simulation results, CERES EBAF produced a decreasing trend in R_c in the North China Plain (32–40°N, 114–121°E) and east China. This might be attributed to the increasing trend in aerosol loading in these areas that is consistent with previous studies (Tang et al., 2017; Yang et al., 2009). ERAI, JRA55, CFSR, and MERRA show overestimated R_c trends in the North China Plain because these reanalyses do not include the increase in aerosols that corresponds a decreasing trend in R_c. ERAI exhibits negative biases in the R_c trend in northern China, and therefore, the uncertainties in the water vapor trend from ERAI might not be ruled out (Ning et al., 2013).

3.3. The Impacts of CF and R_c on Biases in the Mean and Trend of R_s

Figure 6 illustrates the correlation between the annual anomalies of CF, R_c, and annual anomalies of R_s. Based on observations, reanalyses fail to produce the weak negative correlation between the annual

Table 4
Statistical Summary of the Determination Coefficient (R^2) and Sensitivity Between the Bias in the Annual Anomaly Surface Solar Radiation (R_s) and the Bias in the Annual Anomaly Cloud Fraction (CF) Given the National Mean Over China

			Sensitivity		R^2	
	Ref R_s	Ref CF	Mean	Median	Mean	Median
ERAI	Obs	Obs	−102.97 ± 1.78	−102.33 ± 0.40	0.36	0.31
JRA55	Obs	Obs	−83.60 ± 12.80	−85.13 ± 0.50	0.31	0.26
CFSR	Obs	Obs	−115.27 ± 9.95	−104.93 ± 0.29	0.37	0.35
MERRA2	Obs	Obs	−70.46 ± 4.09	−72.72 ± 0.47	0.28	0.23
MERRA	Obs	Obs	−99.03 ± 1.28	−103.92 ± 0.38	0.43	0.42
ERAI	CERES	CERES	−141.89 ± 0.36	−162.46 ± 0.33	0.45	0.50
JRA55	CERES	CERES	−136.48 ± 0.45	−140.97 ± 0.41	0.42	0.44
CFSR	CERES	CERES	−133.93 ± 0.25	−142.74 ± 0.23	0.43	0.44
MERRA2	CERES	CERES	−120.60 ± 0.48	−122.72 ± 0.41	0.41	0.43
MERRA	CERES	CERES	−141.87 ± 0.32	−147.61 ± 0.28	0.55	0.60
ERAI	Obs	CERES	−120.25 ± 0.67	−125.72 ± 0.30	0.34	0.30
JRA55	Obs	CERES	−97.14 ± 0.81	−105.79 ± 0.36	0.29	0.26
CFSR	Obs	CERES	−121.06 ± 0.74	−123.60 ± 0.20	0.35	0.30
MERRA2	Obs	CERES	−90.71 ± 0.52	−90.82 ± 0.32	0.24	0.19
MERRA	Obs	CERES	−116.95 ± 0.55	−123.39 ± 0.25	0.41	0.40

Note. CERES is CERES EBAF data and Obs is observed data. Time span is from 2000 to 2014. CERES EBAF = Clouds and the Earth's Radiant Energy System energy balanced and filled product; MERRA = Modern-Era Retrospective Analysis for Research and Applications; JRA55 = Japanese 55-year reanalysis; ERAI = European Centre for Medium Range Weather Forecasting Reanalysis-Interim; CFSR = Climate Forecast System Reanalysis.

anomalies of CF and R_s in northern China because most reanalyses ignore the interannual variability in dust, which leaves the interannual variability in R_s from reanalyses highly dependent on the CF (Fujiwara et al., 2017; Randles et al., 2017; Zhang et al., 2019). The distribution diagrams of Figure 6 further show that reanalyses have more negative correlation between the CF and R_s than that of observations.

Positive correlations between annual anomalies in R_c and annual anomalies in R_s are found in northern China based on the observations and CERES EBAF data (Figure 6). However, only MERRA2 shows consistent correlation spatial patterns, which is likely because of its improvement in aerosol simulation.

Figure 7 shows the correlation between the bias in annual anomaly CF and the bias in the annual anomaly R_s. Using field observations as reference, reanalyses produce negative correlation between the bias in the annual anomaly CF and that in the annual anomaly R_s, with the national mean determination coefficient (R^2) ranging from 0.36 to 0.43 (Table 4). Figure 7 also show that reanalyses have stronger negative correlation when both CF and R_s reference data use CERES EBAF data. Because R_s and CF are independently observed for the field observations, the CERES EBAF R_s is calculated from its CF. In spatial terms, the negative correlation coefficient between the annual anomaly CF bias and annual anomaly R_s bias is high in southern China (−0.50 to −1.00) and low in northern China (−0.40 to 0.00), compared with field observation. Similar spatial patterns can also be found by using the CERES EBAF data as a reference, excluding MERRA2, which shows a high negative correlation in northeast China.

The sensitivity of the annual anomaly bias in R_s to that in the CF from reanalyses (Figure 8) correspondingly exhibits an almost similar spatial pattern compared with the correlation results from Figure 7. MERRA2 has less sensitivity of the annual bias in R_s to that in the CF than MERRA, ERAI, JRA55, and CFSR because these reanalyes except MERRA2 do not include the impact of interannual variability in aerosols on R_s.

Figure 9 shows the correlation between the bias in annual anomaly R_c and that in the annual anomaly R_s. All reanalyses show an almost positive correlation between the bias in annual anomaly R_c and that in the annual anomaly R_s with national means of R^2 ranging from 0.08 to 0.32 (Table 5). In spatial terms, a high positive correlation coefficient between the bias in the annual anomaly R_c and the bias in the annual anomaly R_s over China can be seen in northern China based on JRA55, CFSR, MERRA2, and MERRA, which is probably because the low CF in northern China has a small impact on the variation in R_s, while aerosols and water vapor have large contributions to the modification of the variation in the annual anomaly R_s in northern China. Comparatively, the ERAI shows a low correlation coefficient between the bias in the annual

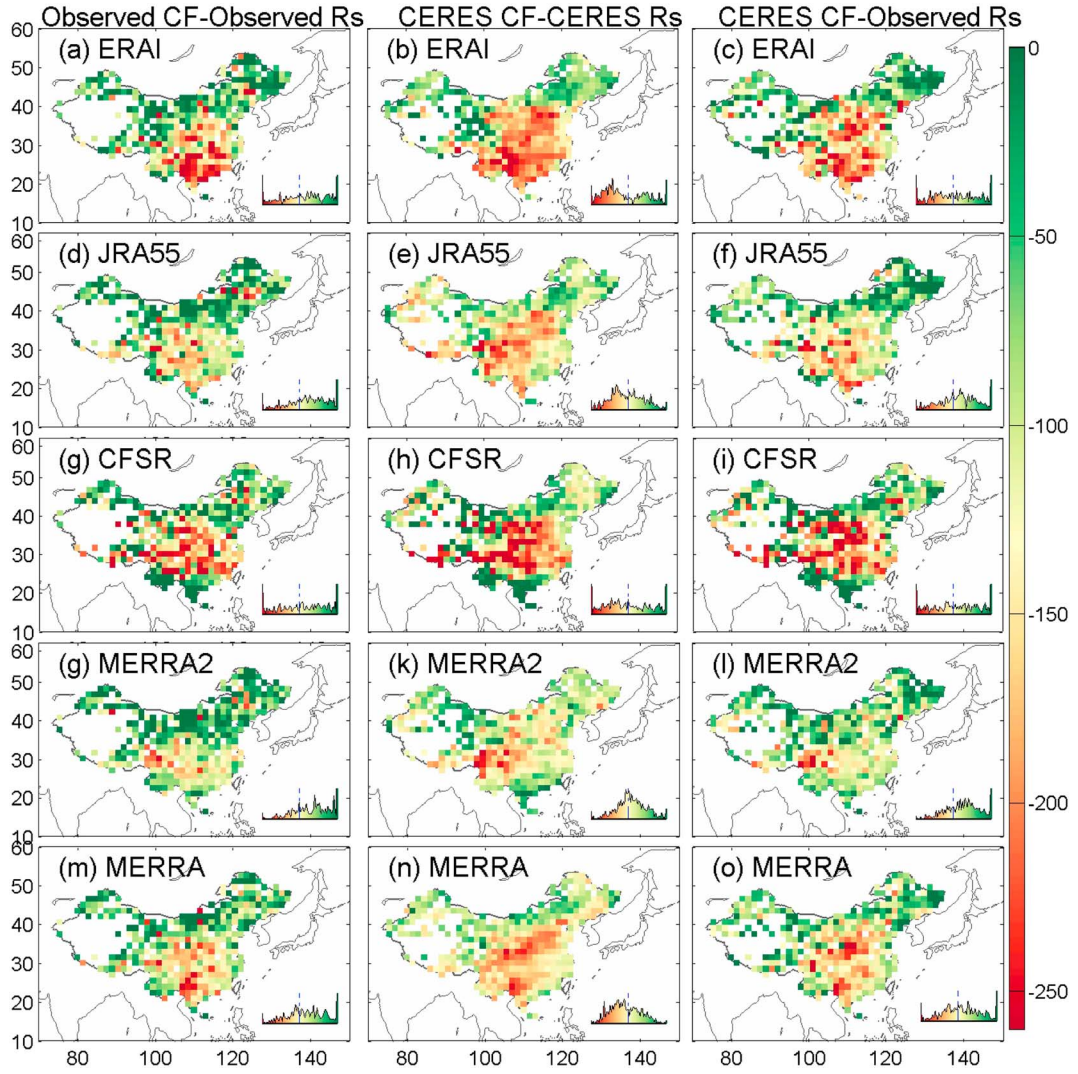

Figure 8. Maps of sensitivity between the bias in the annual anomaly cloud fraction (CF) and the bias in the annual anomaly of surface solar radiation (R_s) for the five reanalyses using various sources as the reference. In the left column (a, d, g, j, and m), the observed CF and the SunDu R_s represent the reference data. In the middle column (b, e, h, k, and n), the CERES CF and CERES R_s represent the reference data. In the right column (c, f, i, l, and o), the CERES CF and the SunDu R_s represent the reference data. The time span is from 2000 to 2014. The probability density plot embedded in each subplot is the same with Figure 2 but stands for the distribution of sensitivity between the bias in the annual anomaly CF and the bias in the annual anomaly of R_s. CERES EBAF = Clouds and the Earth's Radiant Energy System energy balanced and filled product.

anomaly R_c and the bias in the annual anomaly R_s, which might be due to the calculation method for R_c in the ERAI. We calculate the R_c using the ERAI clear-sky net R_s and its forecast albedo product. However, the calculated R_c may be a little different from the R_c data used in the original ERAI radiation transfer calculation (Hogan, 2014).

For the impacts of R_s mean bias, the correlation results (Table 4) show that the biases in the CF in MERRA can largely explain the biases in R_s by 55%, followed by ERAI (45%), CFSR (43%), JRA55 (42%), and MERRA2 (41%) using satellite data as a reference. The biases in R_c can explain the biases in R_s by 32% in JRA55, 29% in MERRA, 22% in CFSR, 14% in MERRA2, and 9% in ERAI using satellite data as a reference (Table 5). The correlation results suggest that the bias in the CF has more impacts on the bias in R_s than that in R_c.

Figure 10 shows the sensitivity of trend error in R_s to that in CF, and Figure 11 illustrate the sensitivity of trend error in R_s to that in R_c. In spatial terms, the trend error in the CF in all five reanalyses (except

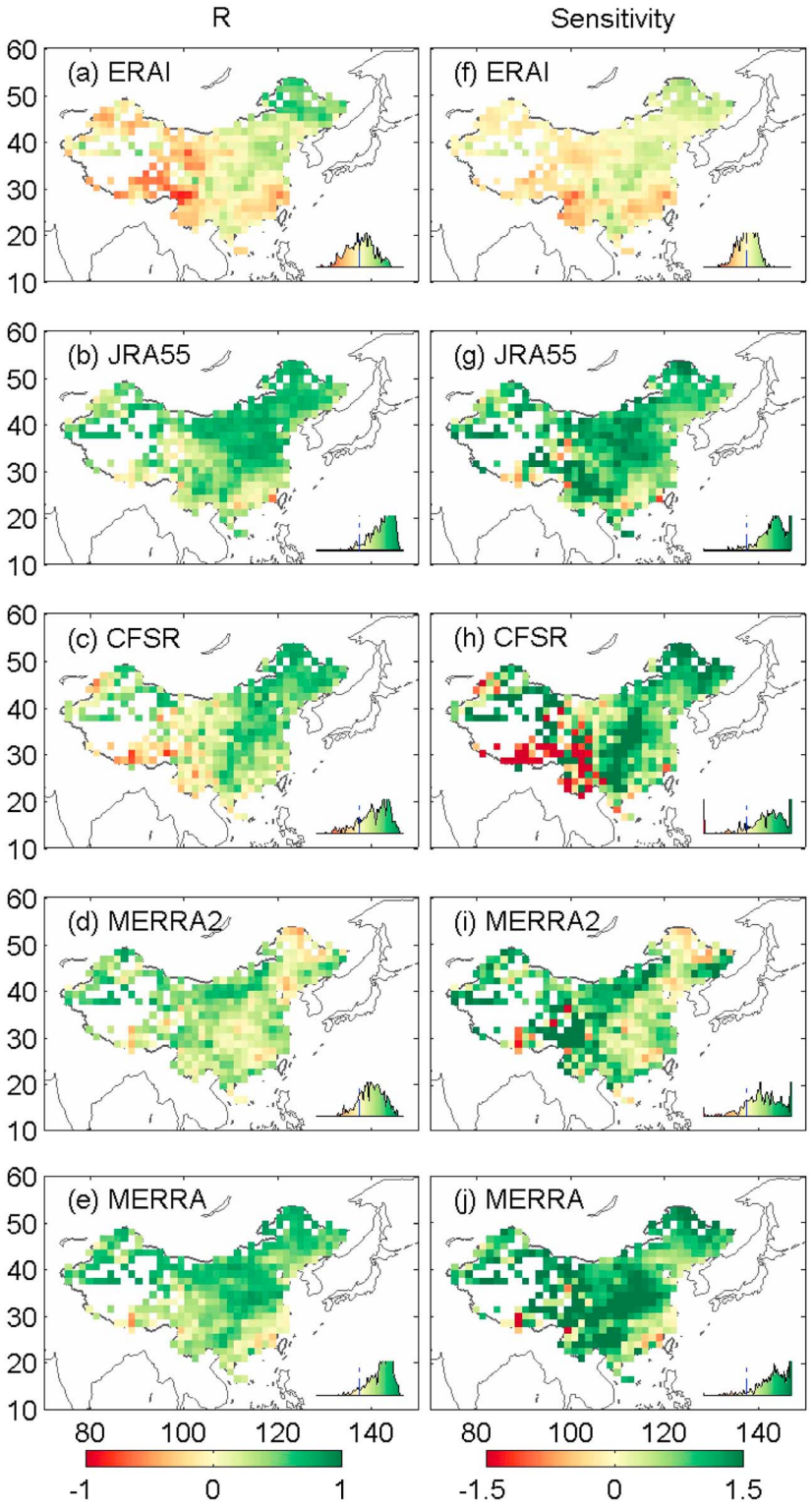

Figure 9. The correlation coefficient (R) between the bias in the annual anomaly surface solar radiation (R_s) and the bias in the annual anomaly surface solar radiation under clear-sky condition (R_c), and sensitivity of the bias in the annual anomaly R_s to the bias in the annual anomaly R_c. The left column (a–e) shows the R, and the right column (f–j) shows the sensitivity. The reference data are the CERES EBAF-derived R_s. The time span is from 2000 to 2014. The probability density plot embedded in each subplot is the same with Figure 2 but stands for the distribution of the correlation coefficient. CERES EBAF = Clouds and the Earth's Radiant Energy System energy balanced and filled product.

Table 5
Statistical Summary of the Determination Coefficient (R^2) and Sensitivity Between the Bias in the Annual Anomaly Surface Solar Radiation (R_s) and the Bias in the Annual Anomaly R_s Under Clear Sky Condition (R_c) Given the National Mean Over China

			Sensitivity		R^2	
	Ref R_s	Ref R_c	Mean	Median	Mean	Median
ERAI	Obs	CERES	−0.04 ± 2.63e−3	−0.04 ± 1.08e−3	0.08	0.04
JRA55	Obs	CERES	0.62 ± 4.65e−3	0.62 ± 2.91e−3	0.17	0.12
CFSR	Obs	CERES	0.25 ± 3.86e−3	0.46 ± 1.79e−3	0.14	0.09
MERRA2	Obs	CERES	0.38 ± 5.47e−3	0.29 ± 3.72e−3	0.09	0.05
MERRA	Obs	CERES	0.79 ± 7.65e−3	0.76 ± 2.25e−3	0.17	0.13
ERAI	CERES	CERES	0.00 ± 1.19e−3	0.03 ± 1.11e−3	0.09	0.05
JRA55	CERES	CERES	0.92 ± 3.70e−3	0.95 ± 3.26e−3	0.32	0.33
CFSR	CERES	CERES	0.60 ± 2.20e−3	0.83 ± 2.01e−3	0.22	0.19
MERRA2	CERES	CERES	0.65 ± 4.45e−3	0.55 ± 4.04e−3	0.14	0.09
MERRA	CERES	CERES	1.07 ± 3.00e−3	1.06 ± 2.52e−3	0.29	0.28

Note. CERES represents the CERES EBAF data, and Obs represents the observed data. The time span is from 2000 to 2014. CERES EBAF = Clouds and the Earth's Radiant Energy System energy balanced and filled product; MERRA = Modern-Era Retrospective Analysis for Research and Applications; JRA55 = Japanese 55-year reanalysis; ERAI = European Centre for Medium Range Weather Forecasting Reanalysis-Interim; CFSR = Climate Forecast System Reanalysis.

MERRA2) can largely explain the trend error in R_s, especially in east China (Figure 10). However, the trend error in R_c in all five reanalyses, except MERRA2 and JRA55, can only slightly explain the trend error in R_s (Figure 11). The distribution diagrams of Figures 10 and 11 further show that the trend error in R_s is more sensitive to that of CF than the trend error in R_c.

In summary, the trend error in the CF from 2000 to 2014 in MERRA can explain the trend error in R_s by 73%, followed by ERAI (64%), CFSR (44%), MERRA2 (35%), and JRA55 (12%) using the CERES EBAF data as a reference (Table 6). The trend error in R_c from 2000 to 2014 can explain the trend error in R_s by 36% in ERAI, 32% in JRA55, 34% in CFSR, 43% in MERRA2, and 30% MERRA using the CERES EBAF data as a reference.

4. Discussion

4.1. Performances of the Reanalyses

Using the best records of historic surface radiation data and trends by Sun duration observed data, this study presents a comprehensive analysis of the performance of five reanalyses commonly used in atmospheric research with regard to geographically distributed surface solar radiation trends over China. Our results show that all five reanalyses are wrong in the same direction with regard to R_s, regardless of the different methods and parameterizations used for CF and aerosols, which are consistent with previous findings (Jia et al., 2013; Wang et al., 2015; Wu et al., 2015; Xia et al., 2006). This is largely because the current climate models have difficulty simulating low-level clouds, such as stratus clouds in southern China (Yu et al., 2001; Yu et al., 2004). High AOD in winter and aerosol-cloud interaction make it worse (Li et al., 2016; Li et al., 2017). Results also demonstrate the dangers of using only radiative transfer and climatological aerosol information without data assimilation in the reanalysis packages

Our sensitivity analyses illustrate that the biases in CF in the reanalyses can explain the biases in R_s by 55–41%, and the biases in R_c can explain the biases in R_s by 32–9%. These two factors together can explain the biases in R_s by 87–50%. The biases in R_s are more sensitive to the CF than those in the R_c in the reanalyses.

The improvement in aerosol simulation of MERRA2 recently draws much attention (Randles et al., 2017). Our previous study (*Feng and Wang*; Wang, 2014) also shows MERRA2 has a better performance in the simulation of the R_s trend and R_c than MERRA, and the correlation between CF and R_s in northern China from MERRA2 is smaller than MERRA. However, the R_s trend error in MERRA2 is still very large because the simulation error of clouds still exists.

CERES EBAF R_s retrievals have been used to compare with the reanalyses. Our previous study also suggests that CERES EBAF R_s retrievals have 9.9 W/m^2 mean absolute biases comparing with BSRN sites data (Feng

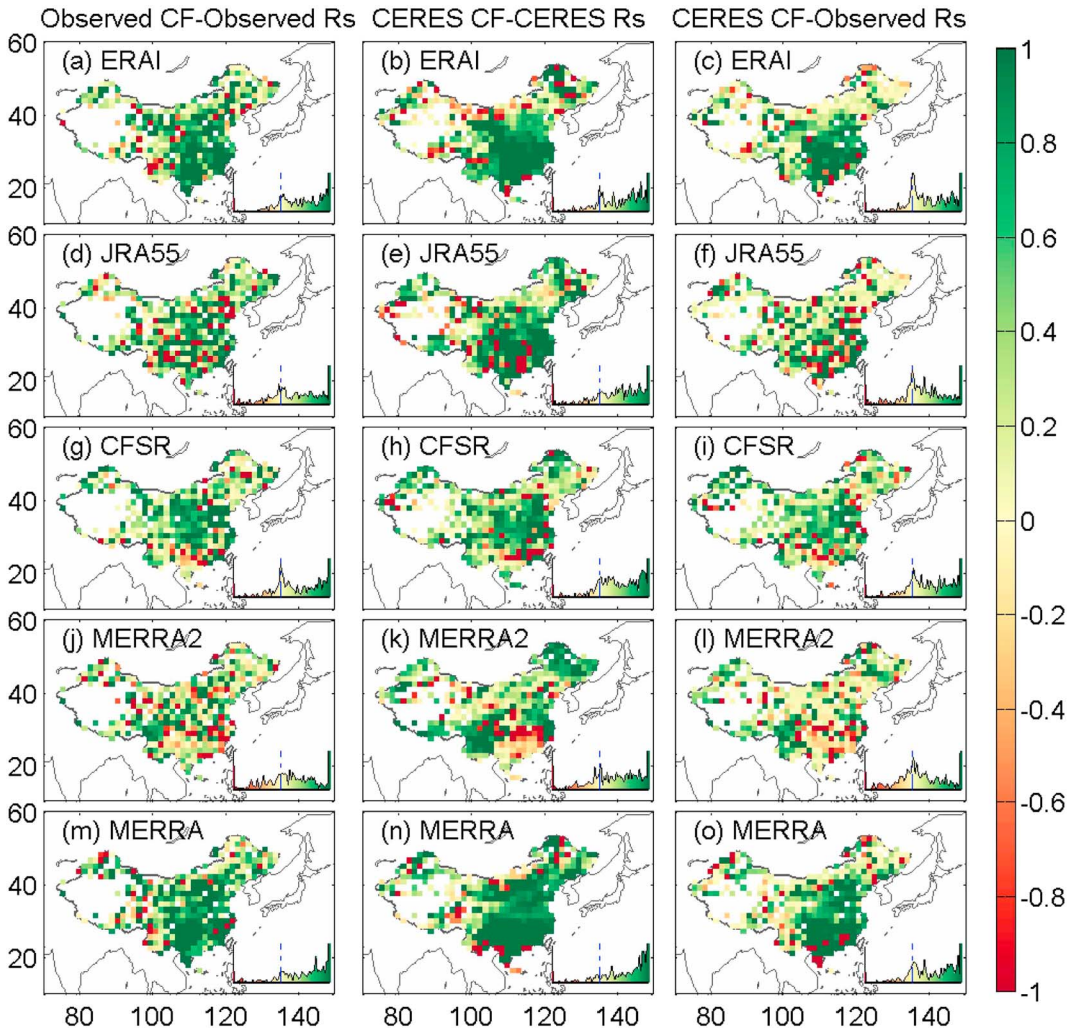

Figure 10. The sensitivity of trend error in annual anomaly surface solar radiation (R_s) to that in the annual anomaly cloud fraction (CF). The left column is calculated based on field observations, the middle column is calculated based on CERES EBAF data, and the right column shows the cross terms. The time span is from 2000 to 2014. The probability density plot embedded in each subplot is the same with Figure 2 but stands for the distribution of the sensitivity of trend error in annual anomaly R_s to that in the annual anomaly CF. CERES EBAF = Clouds and the Earth's Radiant Energy System energy balanced and filled product.

& Wang, 2018b). Existing study suggest that changing the MODIS AOD from Collections 4 to 5 resulted in the discontinuity in the CERES EBAF global land R_s in 2006 (Jia et al., 2018). Moreover, satellite AOD retrievals are only available under cloud-free conditions, which cannot fully represent AOD trend in the all-weather situation. Although upgrades have been made in CERES EBAF data recently, the uncertainties of MODIS AOD trend used in CERES EBAF data might not be ignored. Likewise, the limited number of observations in the west part of China might have potential impacts on the application of the area-weighted method in data-void regions and its uncertainties cannot be ruled out. Moreover, SunDu data are derived from human read of a burned signal. Alternation of human observer should produce inhomogeneous time series of SunDu data. Although the SunDu-derived R_s used in this study is processed carefully with quality control (He et al., 2018; Wang et al., 2015), the uncertainties of SunDu data also cannot be ignored.

4.2. Impact Factors of Variability in R_s

Previous studies (Boers et al., 2017; Pfeifroth et al., 2018; Wang, Dickinson, et al., 2012) have confirmed that clouds and aerosols are the dominant factors in the variation in R_s. Comparatively, radiatively active gases

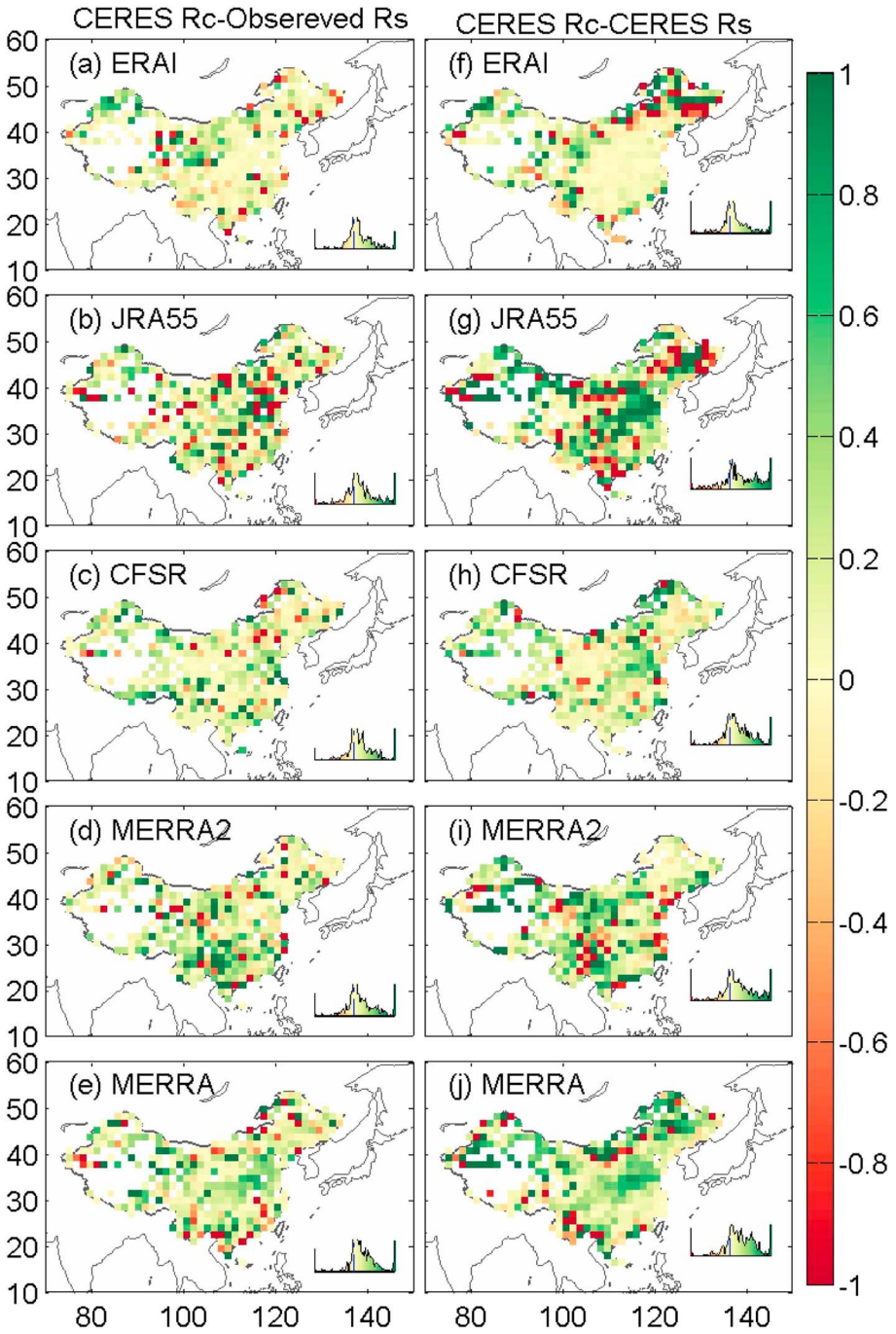

Figure 11. The sensitivity of trend error in annual anomaly surface solar radiation (R_s) to that in the annual anomaly surface solar radiation under clear-sky condition (R_c). In the left column (a–e), the R_s trend bias is calculated based on field observations, and the right column (f–j) is calculated based on CERES EBAF data. The time span is from 2000 to 2014. CERES EBAF = Clouds and the Earth's Radiant Energy System energy balanced and filled product.

and water vapor have minor effects on the variation in R_s (Kvalevåg & Myhre, 2007; Mateos et al., 2013; Wild, 2016) and indicated that aerosols are the main factor affecting the variation in R_c. Large aerosol emissions due to rapid development in China are expected to be the main factor for the variation in R_s over China (Liang & Xia, 2005; Qian et al., 2015; Wang, Yang, et al., 2012). Li et al. (2018) further stated that the variation in single-scattering albedo can also affect the trend in R_s, especially for diffuse radiation. However, the study conducted by Tang et al. (2017) suggests that clouds are likely to be the main contributor to the variation

Table 6
Statistical Summary of Trend Bias Sensitivity Coefficient (i.e., the R_s Trend) Is Explained by the Cloud Fraction (CF) and the Surface Solar Radiation Under Clear-Sky Condition (R_c)

	Explain	R_s_ref	Cloud_ref	Mean	Median
ERAI	Cloud	Obs	Obs	0.55	0.63
JRA55	Cloud	Obs	Obs	0.46	0.45
CFSR	Cloud	Obs	Obs	0.49	0.50
MERRA2	Cloud	Obs	Obs	0.20	0.19
MERRA	Cloud	Obs	Obs	0.81	0.78
ERAI	Cloud	CERES	CERES	0.64	0.69
JRA55	Cloud	CERES	CERES	0.12	0.60
CFSR	Cloud	CERES	CERES	0.44	0.52
MERRA2	Cloud	CERES	CERES	0.35	0.40
MERRA	Cloud	CERES	CERES	0.73	0.88
ERAI	Cloud	Obs	CERES	0.54	0.56
JRA55	Cloud	Obs	CERES	0.51	0.46
CFSR	Cloud	Obs	CERES	0.55	0.55
MERRA2	Cloud	Obs	CERES	0.47	0.38
MERRA	Cloud	Obs	CERES	0.63	0.73
ERAI	R_c	Obs	CERES	0.27	0.17
JRA55	R_c	Obs	CERES	0.23	0.15
CFSR	R_c	Obs	CERES	0.22	0.15
MERRA2	R_c	Obs	CERES	0.32	0.18
MERRA	R_c	Obs	CERES	0.21	0.18
ERAI	R_c	CERES	CERES	0.36	0.23
JRA55	R_c	CERES	CERES	0.32	0.21
CFSR	R_c	CERES	CERES	0.34	0.23
MERRA2	R_c	CERES	CERES	0.43	0.33
MERRA	R_c	CERES	CERES	0.30	0.21

Note. CERES represents the CERES EBAF data, and Obs represents the observed data. The time span is from 2000 to 2014.
CERES EBAF = Clouds and the Earth's Radiant Energy System energy balanced and filled product; MERRA = Modern-Era Retrospective Analysis for Research and Applications; JRA55 = Japanese 55-year reanalysis; ERAI = European Centre for Medium Range Weather Forecasting Reanalysis-Interim; CFSR = Climate Forecast System Reanalysis.

in R_s. The controlling factors of variability in R_s is difficult to qualify, systematic studies including all impact factors may conduct only at site scale or using climate models. All these factors jointly lead to the different conclusions from earlier studies. Therefore, improving the R_s simulation model such as reanalyses is helpful for further studies on this issue.

Atmospheric aerosol loading is fixed in most reanalyses except MERRA2; the major driver of R_c produced by most reanalyses are water vapor. Compared with CERES EBAF, the main error sources of R_c data from reanalyses are mainly aerosol, although water vapor cannot be rule out (Dolinar et al., 2016). This is also true for MERRA2.

Cloud overlap schemes have close relationships with the vertical resolutions in the reanalyses (Oreopoulos & Khairoutdinov, 2003; Stephens et al., 2004), which can also introduce uncertainties in the simulation of CF. Wang et al. (2016) found that there were nonnegligible biases in simulating clouds and their shortwave radiation effects by using a maximum and random overlap scheme. Recently, the newly developed Monte Carlo independent column approximation scheme is expected to have an overwhelming advantage in simulating clouds compared with other cloud overlap schemes.

This study discusses the impacts of CF on R_s in the reanalyses and the contribution of aerosols to R_s variability. Other cloud and aerosol properties might also be important factors, for example, changes in cloud radiative properties, such as cloud optical thickness (Deneke et al., 2008; McCoy et al., 2014). Cloud height, which is relative to the distributions of low clouds, also impacts the variation in R_s (An et al., 2017; Matuszko, 2012). Li et al. (2018) show that the variation in single-scattering albedo has a substantial impact on the trend in R_s.

Moreover, elevation also impacts R_s. For example, comparison results of observed R_s, GEWEX-SRB, and ISCCP-FD in Tibet from Yang et al. (2006) show the differences in elevations and these products might result in nonnegligible uncertainties. Du et al. (2018) also find that the elevation bias in reanalyses has important impacts on temperature biases of reanalyses.

5. Conclusions

Our results show that all reanalyses overestimate the multiyear mean R_s over China (24.10–40.00 W/m^2) and correspondingly underestimate the multiyear mean CF (−0.18 to −0.03) for the highest and lowest of reanalyses, especially in southern China. ERAI and CFSR have a larger bias in simulating R_c compared with those of JRA55, MERRA2, and MERRA. ERAI and CFSR show high positive biases in R_c in south China and negative biases in northwest China. All reanalyses have larger R_s relative biases in winter and spring than other seasons.

We partite the error source between clouds and aerosols and find the biases in the CF can explain the biases in R_s by 41–55%, and the bias in R_c, which is primarily due to errors in atmospheric aerosol loading, can explain 9–32% of the bias in R_s in the reanalyses. The trend error in the CF in the reanalyses can largely explain approximately 12–73% of the trend error in R_s, while the trend error in R_c can explain 30–43% of the trend error in R_s using CERES EBAF as a reference. In east China, the trend error in R_s can be largely explained by those in the CF in the five reanalyses (excluding MERRA2). The trend error in R_c in all five reanalyses have a weak relationship with those in R_s (excluding MERRA2 and JRA55). The biases in R_s are more sensitive to the biases in the CF than those in the R_c. Reanalysis data are commonly used as truth and credible support for atmospheric research; our study suggests that improvement of the cloud and aerosol representation in reanalyses is needed, especially for aerosol-cloud interactions parameterization.

Acknowledgments

This study was funded by the National Natural Science Foundation of China (41525018) and the National Key Research & Development Program of China (2017YFA06036001). We would like to thank Jizeng Du, Yanyi He, Runze Li, Qian Ma, Guocan Wu, and Chunlue Zhou for their insightful comments. The reanalysis data can be downloaded from https://rda.ucar.edu/. The ERAI data can be found at https://rda.ucar.edu/datasets/ds627.1/ and https://www.ecmwf.int/en/forecasts/datasets/reanalysis-datasets/era-interim. The JRA55 data can be found at https://rda.ucar.edu/datasets/ds628.1/ and https://jra.kishou.go.jp/JRA-55/index_en.html. The CFSR data can be found at https://rda.ucar.edu/datasets/ds093.1/. The MERRA data can be found at https://disc.gsfc.nasa.gov/daac-bin/FTPSubset.pl. The MERRA2 data can be found at https://disc.gsfc.nasa.gov/datasets/M2TMNXRAD_V5.12.4/summary?keywords=%22MERRA-2%22.

References

An, N., Wang, K., Zhou, C., & Pinker, R. T. (2017, Observed variability of cloud frequency and cloud-base height within 3600 m above the surface over the Contiguous United States. *Journal of Climate*, *30*(10), 3725–3742. https://doi.org/10.1175/JCLI-D-16-0559.1

Augustine, J. A., & Dutton, E. G. (2013). Variability of the surface radiation budget over the United States from 1996 through 2011 from high-quality measurements. *Journal of Geophysical Research: Atmospheres*, *118*, 43–53. https://doi.org/10.1029/2012JD018551

Bacmeister, J. T., Suarez, M. J., & Robertson, F. R. (2006). Rain Reevaporation, Boundary Layer Convection Interactions, and Pacific Rainfall Patterns in an AGCM, *Journal of the Atmospheric Sciences*, *63*(12), 3383–3403.

Berrisford, P., Dee, D. P., Mark, F., Manuel, F., Kållberg, P. W., Kobayashi, S., & Uppala, S. (2009). The ERA-Interim archive. *ERA Report Series*, *1*(1), 1–16.

Bodas-Salcedo, A., Williams, K. D., Ringer, M. A., Beau, I., Cole, J. N. S., Dufresne, J. L., et al. (2014). Origins of the solar radiation biases over the Southern Ocean in CFMIP2 models. *Journal of Climate*, *27*(1), 41–56. https://doi.org/10.1175/JCLI-D-13-00169.1

Boers, R., Brandsma, T., & Siebesma, A. P. (2017). Impact of aerosols and clouds on decadal trends in all-sky solar radiation over the Netherlands (1966-2015). *Atmospheric Chemistry and Physics*, *17*(13), 8081–8100. https://doi.org/10.5194/acp-17-8081-2017

Briegleb, B. P. (1992). Delta-Eddington approximation for solar radiation in the NCAR community climate model. *Journal of Geophysical Research*, *97*(D7), 7603–7612. https://doi.org/10.1029/92JD00291

Che, H. Z., Shi, G. Y., Zhang, X. Y., Arimoto, R., Zhao, J. Q., Xu, L., et al. (2005). Analysis of 40 years of solar radiation data from China, 1961–2000. *Geophysical Research Letters*, *1029*, L06803. https://doi.org/10.1029/2004GL022322

Clough, S. A., Shephard, M. W., Mlawer, E. J., Delamere, J. S., Iacono, M. J., Cady-Pereira, K., et al. (2005). Atmospheric radiative transfer modeling: A summary of the AER codes. *Journal of Quantitative Spectroscopy and Radiative*, *91*(2), 233–244. https://doi.org/10.1016/j.jqsrt.2004.05.058

Dee, D., Uppala, S., Simmons, A., Berrisford, P., Poli, P., Kobayashi, S., et al. (2011). The ERA-Interim reanalysis: Configuration and performance of the data assimilation system. *Quarterly Journal of the Royal Meteorological Society*, *137*(656), 553–597. https://doi.org/10.1002/qj.828

Deneke, H. M., Feijt, A. J., & Roebeling, R. A. (2008). Estimating surface solar irradiance from METEOSAT SEVIRI-derived cloud properties. *Remote Sensing of Environment*, *112*(6), 3131–3141. https://doi.org/10.1016/j.rse.2008.03.012

Dolinar, E. K., Dong, X., & Xi, B. (2016). Evaluation and intercomparison of clouds, precipitation, and radiation budgets in recent reanalyses using satellite-surface observations. *Climate Dynamics*, *46*(7-8), 2123–2144. https://doi.org/10.1007/s00382-015-2693-z

Dorno, C. (1920). On observations of solar and sky radiations and their importance to climatology and biology and also to geophysics and astronomy. *Monthly Weather Review*, *48*(1), 18–24. https://doi.org/10.1175/1520-0493(1920)48<18:OOOSAS>2.0.CO;2

Du, J., Wang, K. C., Wang, J., Jiang, S., & Zhou, C. (2018). Diurnal cycle of surface air temperature within China in current reanalyses: Evaluation and diagnostics. *Journal of Climate*, *31*(11), 4585–4603. https://doi.org/10.1175/JCLI-D-17-0773.1

Essou, G. R. C., Brissette, F., & Lucas-Picher, P. (2017). The use of reanalyses and gridded observations as weather input data for a hydrological model: Comparison of performances of simulated river flows based on the density of weather stations. *Journal of Hydrometeorology*, *18*(2), 497–513. https://doi.org/10.1175/JHM-D-16-0088.1

Feng, F., & Wang, K. C. (2018a). Does the Modern-Era Retrospective Analysis for Research and Applications-2 aerosol reanalysis introduce an improvement in the simulation of surface solar radiation over China? *International Journal of Climatology*, *39*(3), 1305–1318.

Feng, F., & Wang, K. C. (2018b). Merging satellite retrievals and reanalyses to produce global long-term and consistent surface incident solar radiation datasets. *Remote Sensing*, *10*, 115. https://doi.org/10.3390/rs10010115

Folini, D., & Wild, M. (2011). Aerosol emissions and dimming/brightening in Europe: Sensitivity studies with ECHAM5-HAM. *Journal of Geophysical Research*, *116*, D21104. https://doi.org/10.1029/2011JD016227

Fouquart, Y., & Bonnel, B. (1980). Computation of solar heating of the Earth's atmosphere: A new parameterization. *Beitrage zur Physik der Atmosphare*, *53*, 35–62.

Fujiwara, M., Wright, J. S., Manney, G. L., Gray, L. J., Anstey, J., Birner, T., et al. (2017). Introduction to the SPARC Reanalysis Intercomparison Project (S-RIP) and overview of the reanalysis systems. *Atmospheric Chemistry and Physics*, *17*(2), 1417–1452. https://doi.org/10.5194/acp-17-1417-2017

Gelaro, R., Mccarty, W., Suárez, M. J., Todling, R., Molod, A., Takacs, L., et al. (2017). The Modern-Era Retrospective Analysis for Research and Applications, Version 2 (MERRA-2). *Journal of Climate*, *30*(14), 5419–5454. https://doi.org/10.1175/JCLI-D-16-0758.1

Ghan, S. J., Liu, X., Easter, R. C., Zaveri, R., Rasch, P. J., Yoon, J. H., & Eaton, B. (2012). Toward a minimal representation of aerosols in climate models: Comparative decomposition of aerosol direct, semidirect, and indirect radiative forcing. *Journal of Climate*, *25*(19), 6461–6476. https://doi.org/10.1175/JCLI-D-11-00650.1

He, Y., Wang, K., Zhou, C., & Wild, M. (2018). A revisit of global dimming and brightening based on the sunshine duration. *Geophysical Research Letters*, *45*, 4281–4289. https://doi.org/10.1029/2018GL077424

Hogan, C. R. (2014), Radiation quantities in the ECMWF model and MARS, edited, pp. 1–9.

Jia, A., Liang, S., Jiang, B., Zhang, X., & Wang, G. (2018). Comprehensive assessment of global surface net radiation products and uncertainty analysis. *Journal of Geophysical Research: Atmospheres*, *123*, 1970–1989. https://doi.org/10.1002/2017JD027903

Jia, B., Xie, Z., Dai, A., Shi, C., & Chen, F. (2013). Evaluation of satellite and reanalysis products of downward surface solar radiation over East Asia: Spatial and seasonal variations. *Journal of Geophysical Research: Atmospheres*, *118*, 3431–3446. https://doi.org/10.1002/jgrd.50353

Kato, S., Rose, F. G., Rutan, D. A., Thorsen, T. J., Loeb, N. G., Doelling, D. R., et al. (2018). Surface irradiances of Edition 4.0 Clouds and the Earth's Radiant Energy System (CERES) Energy Balanced and Filled (EBAF) data product. *Journal of Climate*, *31*(11), 4501–4527.

Kobayashi, S., Ota, Y., Harada, Y., Ebita, A., Moriya, M., Onoda, H., et al. (2015). The JRA-55 Reanalysis: General specifications and basic characteristics. *Journal of the Meteorological Society of Japan*, *93*(1), 5–48. https://doi.org/10.2151/jmsj.2015-001

Kvalevåg, M. M., & Myhre, G. (2007). Human impact on direct and diffuse solar radiation during the industrial era. *Journal of Climate*, *20*(19), 4874–4883. https://doi.org/10.1175/JCLI4277.1

Li, J., Jiang, Y. W., Xia, X. G., & Hu, Y. Y. (2018). Increase of surface solar irradiance across East China related to changes in aerosol properties during the past decade. *Environmental Research Letters*, *13*(3). https://doi.org/10.1088/1748-9326/aaa35a

Li, J., Wang, W.-C., Dong, X., & Mao, J. (2017). Cloud-radiation-precipitation associations over the Asian monsoon region: an observational analysis. *Climate Dynamics*, *49*(9-10), 3237–3255. https://doi.org/10.1007/s00382-016-3509-5

Li, X., Xin, X., & Peng, Z. (2017). Change analysis of surface solar radiation In China from 2003 to 2012. *Acta Energiae Solaris Sinica*, *38*(11), 3057–3066.

Li, Z., Lau, W. K. M., Ramanathan, V., Wu, G., Ding, Y., Manoj, M. G., et al. (2016). Aerosol and monsoon climate interactions over Asia. *Reviews of Geophysics*, *54*, 866–929. https://doi.org/10.1002/2015RG000500

Liang, F., & Xia, X. A. (2005). Long-term trends in solar radiation and the associated climatic factors over China for 1961-2000. *Annales Geophysicae*, *23*(7), 2425–2432. https://doi.org/10.5194/angeo-23-2425-2005

Loew, A., Andersson, A., Trentmann, J., & Schröder, M. (2016). Assessing surface solar radiation fluxes in the CMIP ensembles. *Journal of Climate*, *29*(20), 7231–7246. https://doi.org/10.1175/jcli-d-14-00503.1

Ma, Q., Wang, K. C., & Wild, M. (2015). Impact of geolocations of validation data on the evaluation of surface incident shortwave radiation from Earth System Models. *Journal of Geophysical Research: Atmospheres*, *120*, 6825–6844. https://doi.org/10.1002/2014JD022572

Manara, V., Beltrano, M. C., Brunetti, M., Maugeri, M., Sanchez-Lorenzo, A., Simolo, C., & Sorrenti, S. (2015). Sunshine duration variability and trends in Italy from homogenized instrumental time series (1936–2013). *Journal of Geophysical Research: Atmospheres*, *120*, 3622–3641. https://doi.org/10.1002/2014JD022560

Mateos, D., Antón, M., Sanchez-Lorenzo, A., Calbó, J., & Wild, M. (2013). Long-term changes in the radiative effects of aerosols and clouds in a mid-latitude region (1985–2010). *Global and Planetary Change*, *111*, 288–295. https://doi.org/10.1016/j.gloplacha.2013.10.004

Matuszko, D. (2012). Influence of the extent and genera of cloud cover on solar radiation intensity. *International Journal of Climatology*, *32*(15), 2403–2414. https://doi.org/10.1002/joc.2432

Matuszko, D. (2014). Long-term variability in solar radiation in Krakow based on measurements of sunshine duration. *International Journal of Climatology*, *34*(1), 228–234. https://doi.org/10.1002/joc.3681

McCoy, D. T., Hartmann, D. L., & Grosvenor, D. P. (2014). Observed Southern Ocean cloud properties and shortwave reflection. Part I: Calculation of SW flux from observed cloud properties. *Journal of Climate*, *27*(23), 8836–8857. https://doi.org/10.1175/jcli-d-14-00287.1

Molod, A., Takacs, L., Suarez, M., & Bacmeister, J. (2015). Development of the GEOS-5 atmospheric general circulation model: Evolution from MERRA to MERRA2. *Geoscientific Model Development*, *8*(5), 1339–1356. https://doi.org/10.5194/gmd-8-1339-2015

Myers, D. R., Stoffel, T. L., Reda, I., Wilcox, S. M., & Andreas, A. M. (2002). Recent progress in reducing the uncertainty in and improving pyranometer calibrations. *Journal of Solar Energy Engineering*, *124*(1), 44–50. https://doi.org/10.1115/1.1434262

Nabat, P., Somot, S., Mallet, M., Sanchez-Lorenzo, A., & Wild, M. (2015). Contribution of anthropogenic sulfate aerosols to the changing Euro-Mediterranean climate since 1980. *Geophysical Research Letters*, *41*, 5605–5611.

Ning, T., Elgered, G., Willén, U., & Johansson, J. M. (2013). Evaluation of the atmospheric water vapor content in a regional climate model using ground-based GPS measurements. *Journal of Geophysical Research: Atmospheres*, *118*, 329–339. https://doi.org/10.1029/2012JD018053

Oreopoulos, L., & Khairoutdinov, M. (2003). Overlap properties of clouds generated by a cloud-resolving model. *Journal of Geophysical Research*, *108*(D15), 4479. https://doi.org/10.1029/2002jd003329

Pfeifroth, U., Bojanowski, J. S., Clerbaux, N., Manara, V., Sanchez-Lorenzo, A., Trentmann, J., et al. (2018). Satellite-based trends of solar radiation and cloud parameters in Europe. *Advance Science Research*, *15*, 31–37. https://doi.org/10.5194/asr-15-31-2018

Philipona, R. (2002). Underestimation of solar global and diffuse radiation measured at Earth's surface. *Journal of Geophysical Research*, *107*(D22), 4654. https://doi.org/10.1029/2002JD002396

Pyrina, M., Hatzianastassiou, N., Matsoukas, C., Fotiadi, A., Papadimas, C. D., Pavlakis, K. G., & Vardavas, I. (2015). Cloud effects on the solar and thermal radiation budgets of the Mediterranean basin. *Atmospheric Research*, *152*, 14–28. https://doi.org/10.1016/j.atmosres.2013.11.009

Qian, Y., Kaiser, D. P., Leung, L. R., & Xu, M. (2015). More frequent cloud-free sky and less surface solar radiation in China from 1955 to 2000. *Geophysical Research Letters*, *33*, 311–330. https://doi.org/10.1029/2005GL024586

Ramanathan, V., Chung, C., Kim, D., Bettge, T., Buja, L., Kiehl, J. T., et al. (2005). Atmospheric brown clouds: Impacts on South Asian climate and hydrological cycle. *Proceedings of the National Academy of Sciences of the United States of America*, *102*(15), 5326–5333. https://doi.org/10.1073/pnas.0500656102

Randles, C. A., da Silva, A. M., Buchard, V., Colarco, P. R., Darmenov, A., Govindaraju, R., et al. (2017). The MERRA-2 aerosol reanalysis, 1980 onward. Part I: System description and data assimilation evaluation. *Journal of Climate.*, *30*(17), 6823–6850. https://doi.org/10.1175/jcli-d-16-0609.1

Rienecker, M. M., Suarez, M. J., Gelaro, R., Todling, R., Bacmeister, J., Liu, E., et al. (2011). MERRA: NASA's Modern-Era Retrospective Analysis for Research and Applications. *Journal of Climate.*, *24*(14), 3624–3648. https://doi.org/10.1175/jcli-d-11-00015.1

Roderick, M. L., & Farquhar, G. D. (2002). The cause of decreased pan evaporation over the past 50 years. *Science*, *298*(5597), 1410–1411.

Ruckstuhl, C., Philipona, R., Behrens, K., Collaud Coen, M., Dürr, B., Heimo, A., et al. (2008). Aerosol and cloud effects on solar brightening and the recent rapid warming. *Geophysical Research Letters*, *35*, L12708. https://doi.org/10.1029/2008GL034228

Ruosteenoja, K., & Raisanen, P. (2013). Seasonal changes in solar radiation and relative humidity in Europe in response to global warming. *Journal of Climate.*, *26*(8), 2467–2481. https://doi.org/10.1175/JCLI-D-12-00007.1

Saha, S., Moorthi, S., Pan, H. L., Wu, X., Wang, J., Nadiga, S., et al. (2010). The NCEP climate forecast system reanalysis. *Bulletin of the American Meteorological Society*, *91*(8), 1015–1058. https://doi.org/10.1175/2010BAMS3001.1

Saha, S., Moorthi, S., Wu, X., Wang, J., Nadiga, S., Tripp, P., et al. (2014). The NCEP Climate Forecast System Version 2. *Journal of Climate.*, *27*(6), 2185–2208. https://doi.org/10.1175/jcli-d-12-00823.1

Saha, S., Nadiga, S., Thiaw, C., Wang, J., Wang, W., Zhang, Q., et al. (2006). The NCEP Climate Forecast System. *Journal of Climate.*, *19*(15), 3483–3517. https://doi.org/10.1175/jcli3812.1

Sanchezlorenzo, A., Azorinmolina, C., Wild, M., Vicenteserrano, S. M., Lópezmoreno, J. I., & Corellcustardoy, D. (2013). Feasibility of sunshine duration records to detect changes in atmospheric turbidity: A case study in Valencia (Spain). *American Institute of Physics*, *736-739*.

Sanchez-Lorenzo, A., Calbó, J., Brunetti, M., & Deser, C. (2009). Dimming/brightening over the Iberian Peninsula: Trends in sunshine duration and cloud cover and their relations with atmospheric circulation. *Journal of Geophysical Research*, *114*, D00D09. https://doi.org/10.1029/2008JD011394

Sanchez-Lorenzo, A., Calbo, J., & Martin-Vide, J. (2008). Spatial and temporal trends in sunshine duration over western Europe (1938–2004). *Journal of Climate*, *21*(22), 6089–6098. https://doi.org/10.1175/2008jcli2442.1

Sedlar, J. (2018). Spring Arctic atmospheric preconditioning: Do not rule out shortwave radiation just yet. *Journal of Climate.*, *31*(11), 4225–4240. https://doi.org/10.1175/jcli-d-17-0710.1

Sellers, P. J., Rasool, S. I., & Bolle, H. J. (1990). A review of satellite data algorithms for studies of the land surface. *Bulletin of the American Meteorological Society*, *71*(10), 1429–1447. https://doi.org/10.1175/1520-0477(1990)071<1429:AROSDA>2.0.CO;2

Slater, A. G. (2016). Surface solar radiation in North America: A comparison of observations, reanalyses, satellite, and derived products. *Journal of Hydrometeorology*, *17*(1), 401–420. https://doi.org/10.1175/JHM-D-15-0087.1

Smith, R. N. B. (2010). A scheme for predicting layer clouds and their water content in a general circulation model. *Quarterly Journal of the Royal Meteorological Society*, *116*(492), 435–460.
Stephens, G. L., Wood, N. B., & Gabriel, P. M. (2004). An assessment of the parameterization of subgrid-scale cloud effects on radiative transfer. Part I: Vertical Overlap. *Journal of the Atmospheric Sciences*, *61*(6), 715–732. https://doi.org/10.1175/1520-0469(2004)061<0715:AAOTPO>2.0.CO;2
Tang, Q. H., Leng, G. Y., & Groisman, P. Y. (2012). European hot summers associated with a reduction of cloudiness. *Journal of Climate*, *25*(10), 3637–3644. https://doi.org/10.1175/jcli-d-12-00040.1
Tang, W., Yang, K., Qin, J., Niu, X., Lin, C., & Jing, X. (2017). A revisit to decadal change of aerosol optical depth and its impact on global radiation over China. *Atmospheric Environment*, *150*(2), 106–115.
Tang, W. J., Yang, K., Qin, J., Cheng, C. C. K., & He, J. (2011). Solar radiation trend across China in recent decades: A revisit with quality-controlled data. *Atmospheric Chemistry and Physics*, *11*(1), 393–406. https://doi.org/10.5194/acp-11-393-2011
Wang, J., Dong, J., Wang, S., Zhang, L., He, H., Yi, Y., et al. (2017). Decreasing net primary production due to drought and slight decreases in solar radiation in China from 2000 to 2012. *Journal of Geophysical Research: Atmospheres*, *122*, 261–278. https://doi.org/10.1002/2016JG003417
Wang, K. (2014). Measurement biases explain discrepancies between the observed and simulated decadal variability of surface incident solar radiation. *Scientific Reports*, *4*, 6144.
Wang, K., & Dickinson, R. E. (2013). Contribution of solar radiation to decadal temperature variability over land. *Proceedings of the National Academy of Sciences of the United States of America*, *110*(37), 14,877–14,882. https://doi.org/10.1073/pnas.1311433110
Wang, K. C., Dickinson, R. E., Wild, M., & Liang, S. (2012). Atmospheric impacts on climatic variability of surface incident solar radiation. *Atmospheric Chemistry and Physics*, *12*(20), 9581–9592. https://doi.org/10.5194/acp-12-9581-2012
Wang, K. C., Ma, Q., Li, Z., & Wang, J. (2015). Decadal variability of surface incident solar radiation over China: Observations, satellite retrievals, and reanalyses. *Journal of Geophysical Research: Atmospheres*, *120*, 6500–6514. https://doi.org/10.1002/2015JD023420
Wang, X., Liu, Y., & Bao, Q. (2016). Impacts of cloud overlap assumptions on radiative budgets and heating fields in convective regions. *Atmospheric Research*, *167*, 89–99. https://doi.org/10.1016/j.atmosres.2015.07.017
Wang, Y., Yang, Y., Zhao, N., Liu, C., & Wang, Q. (2012). The magnitude of the effect of air pollution on sunshine hours in China. *Journal of Geophysical Research*, *117*, D00V14. https://doi.org/10.1029/2011JD016753
Wild, M. (2009). Global dimming and brightening: A review. *Journal of Geophysical Research*, *114*, D00D16. https://doi.org/10.1029/2008JD011470
Wild, M. (2016). Decadal changes in radiative fluxes at land and ocean surfaces and their relevance for global warming. *Wiley Interdisciplinary Reviews Climate Change*, *7*(1), 91–107. https://doi.org/10.1002/wcc.372
Wood, J. D., Griffis, T. J., & Baker, J. M. (2015). Detecting drift bias and exposure errors in solar and photosynthetically active radiation data, Agr. *Forest Meteorology*, *206*, 33–44. https://doi.org/10.1016/j.agrformet.2015.02.015
Wu, X., W. Ju, Y. Zhou, B. Zhou, and Y. Liu (2015), Evaluation of downward surface solar radiation of three reanalysis products over China from 1979 to 2008, Engineering Technology, Engineering Education and Engineering Management, DOI: https://doi.org/10.1201/b18566-144.
Xia, X. (2010). Spatiotemporal changes in sunshine duration and cloud amount as well as their relationship in China during 1954–2005. *Journal Geophysical Research*, *115*, D00K06. https://doi.org/10.1029/2009JD012879
Xia, X. A., Wang, P. C., Chen, H. B., & Liang, F. (2006). Analysis of downwelling surface solar radiation in China from National Centers for Environmental Prediction reanalysis, satellite estimates, and surface observations. *Journal of Geophysical Research*, *111*, D09103. https://doi.org/10.1029/2005JD006405
Yang, K., Koike, T., Stackhouse, P., Mikovitz, C., & Cox, S. J. (2006). An assessment of satellite surface radiation products for highlands with Tibet instrumental data. *Geophysical Research Letters*, *33*, L22403. https://doi.org/10.1029/2006GL027640
Yang, K., Koike, T., & Ye, B. (2006). Improving estimation of hourly, daily, and monthly solar radiation by importing global data sets. *Agricultural and Forest Meteorology*, *137*(1–2), 43–55. https://doi.org/10.1016/j.agrformet.2006.02.001
Yang, S., Wang, X. L., & Wild, M. (2018). Homogenization and trend analysis of the 1958–2016 in situ surface solar radiation records in China. *Journal of Climate*, *31*(11), 4529–4541. https://doi.org/10.1175/jcli-d-17-0891.1
Yang, Y. H., Zhao, N., Hao, X. H., & Li, C. Q. (2009). Decreasing trend of sunshine hours and related driving forces in north China. *Theoretical and Applied Climatology*, *97*(1-2), 91–98. https://doi.org/10.1007/s00704-008-0049-x
Yu, R., Wang, B., & Zhou, T. (2004). Climate effects of the deep continental stratus clouds generated by the Tibetan Plateau. *Journal of Climate*, *17*(13), 2702–2713. https://doi.org/10.1175/1520-0442(2004)017<2702:CEOTDC>2.0.CO;2
Yu, R. C., Yu, Y. Q., & Zhang, M. H. (2001). Comparing cloud radiative properties between the eastern China and the Indian monsoon region. *Advances in Atmospheric Sciences*, *18*(6), 1090–1102.
Zadra, A., Williams, K., Frassoni, A., Rixen, M., Adames, Á. F., Berner, J., et al. (2018). Systematic errors in weather and climate models: Nature, origins, and Ways Forward. *Bulletin of the American Meteorological Society*, *99*(4), ES67–ES70. https://doi.org/10.1175/bams-d-17-0287.1
Zhang, W. M., & Lu, Z. H. (1988). Technical report on telemering radiometer. *Meteorol Mon*, *14*(7), 20–23.
Zhang, W. M., & Lu, Z. H. (1990). Introduction to telemetry radiation instruments and methods of observation. *Meteorol Mon*, *16*(8), 53–55.
Zhang, X.-X., Sharratt, B., Lei, J. Q., Wu, C. L., Zhang, J., Zhao, C., et al. (2019). Parameterization schemes on dust deposition in northwest China: Model validation and implications for the global dust cycle. *Atmospheric Environment*, *209*, 1–13. https://doi.org/10.1016/j.atmosenv.2019.04.017
Zhou, X., Weiliang, L. I., Chen, L., & Liu, Y. (2006). Study on ozone change over the Tibetan Plateau. *Acta Meteorologica*, *20*(2), 129–143.
Zo, I.-S., Jee, J.-B., Kim, B.-Y., & Lee, K. (2017). Analysis of the thermal dome effect from global solar radiation observed with a modified pyranometer. *Current Optics and Photonics*, *1*, 263–270. https://doi.org/10.3807/COPP.2017.1.4.263